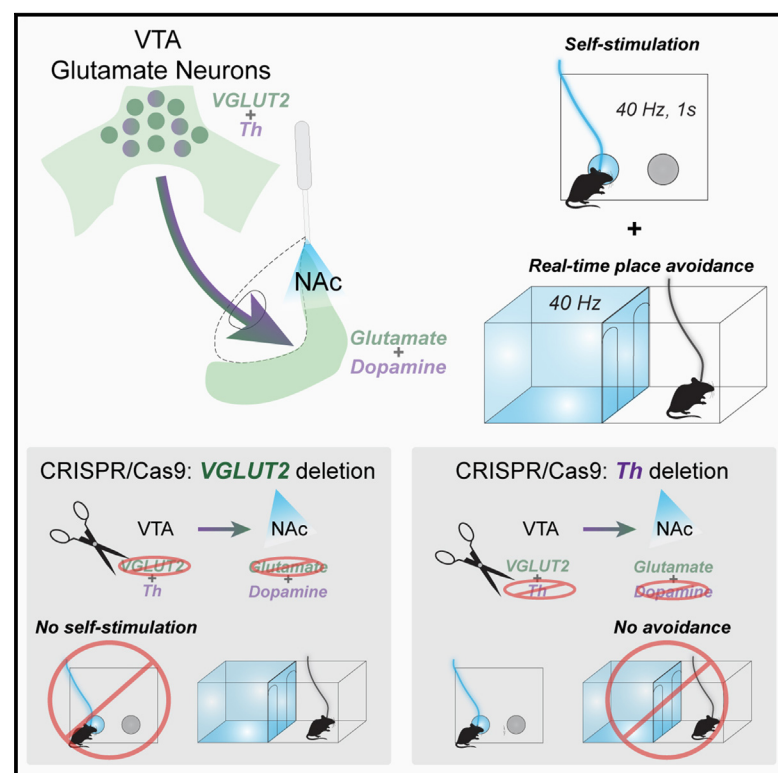


# Mesoaccumbal glutamate neurons drive reward via glutamate release but aversion via dopamine co-release

## Graphical abstract



## Authors

Shelley M. Warlow, Sarthak M. Singhal, Nick G. Hollon, ..., Avery C. Hunker, Larry S. Zweifel, Thomas S. Hnasko

## Correspondence

thnasko@health.ucsd.edu

## In brief

VTA glutamate neurons co-release glutamate and dopamine in the nucleus accumbens, and their activation is associated with both positive reinforcement and aversion. Warlow et al. demonstrate that disrupting glutamate release from VTA glutamate neurons selectively abolishes positive reinforcement, whereas disrupting their ability to co-release dopamine selectively abolishes place aversion.

## Highlights

- VTA glutamate/dopamine neurons are activated by aversive and appetitive stimuli
- Activation of VTA glutamate neurons is reinforcing and aversive
- Glutamate released from VTA glutamate neurons is reinforcing
- Dopamine co-released from VTA glutamate neurons is aversive

Article

# Mesoaccumbal glutamate neurons drive reward via glutamate release but aversion via dopamine co-release

Shelley M. Warlow,<sup>1</sup> Sarthak M. Singhal,<sup>1</sup> Nick G. Hollon,<sup>2</sup> Lauren Faget,<sup>1</sup> Dina S. Dowlat,<sup>1</sup> Vivien Zell,<sup>1</sup> Avery C. Hunker,<sup>3</sup> Larry S. Zweifel,<sup>3</sup> and Thomas S. Hnasko<sup>1,4,5,\*</sup>

<sup>1</sup>Department of Neurosciences, University of California, San Diego, La Jolla, CA, USA

<sup>2</sup>Department of Psychiatry, University of California, San Diego, La Jolla, CA, USA

<sup>3</sup>Department of Pharmacology, University of Washington, Seattle, WA, USA

<sup>4</sup>Veterans Affairs San Diego Healthcare System, San Diego, CA, USA

<sup>5</sup>Lead contact

\*Correspondence: [thnasko@health.ucsd.edu](mailto:thnasko@health.ucsd.edu)

<https://doi.org/10.1016/j.neuron.2023.11.002>

## SUMMARY

Ventral tegmental area (VTA) projections to the nucleus accumbens (NAc) drive reward-related motivation. Although dopamine neurons are predominant, a substantial glutamatergic projection is also present, and a subset of these co-release both dopamine and glutamate. Optogenetic stimulation of VTA glutamate neurons not only supports self-stimulation but can also induce avoidance behavior, even in the same assay. Here, we parsed the selective contribution of glutamate or dopamine co-release from VTA glutamate neurons to reinforcement and avoidance. We expressed channelrhodopsin-2 (ChR2) in mouse VTA glutamate neurons in combination with CRISPR-Cas9 to disrupt either the gene encoding vesicular glutamate transporter 2 (VGLUT2) or tyrosine hydroxylase (*Th*). Selective disruption of VGLUT2 abolished optogenetic self-stimulation but left real-time place avoidance intact, whereas CRISPR-Cas9 deletion of *Th* preserved self-stimulation but abolished place avoidance. Our results demonstrate that glutamate release from VTA glutamate neurons is positively reinforcing but that dopamine release from VTA glutamate neurons can induce avoidance behavior.

## INTRODUCTION

As a principal region within mesocorticolimbic circuitry, the ventral tegmental area (VTA) significantly regulates reward-related motivation, aversion, and cognition. The VTA is a heterogeneous structure containing dopamine, GABA and glutamate neurons, and neurons containing multiple neurotransmitters.<sup>1–4</sup> Indeed, a subset of VTA dopamine neurons projecting to the medial nucleus accumbens (NAc) shell also express the vesicular glutamate transporter 2 (VGLUT2) and release glutamate at NAc terminals.<sup>5–9</sup>

Optogenetic stimulation of VGLUT2-expressing VTA neurons and their projections to medial NAc shell, lateral habenula, or ventral pallidum can promote positive reinforcement. For example, in self-stimulation assays, mice will perform instrumental actions such as nose poking or lever pressing to receive optogenetic stimulation of VTA glutamate neurons, suggesting that increases in their activity are rewarding.<sup>10,11</sup> Self-stimulation of VGLUT2<sup>+</sup> VTA neurons persists despite manipulations that abolish concomitant dopamine release,<sup>12</sup> suggesting that dopamine co-release is not necessary for positive reinforcement

mediated by VTA glutamate neurons. However, it has remained unknown whether glutamate release from VGLUT2<sup>+</sup> VTA neurons is required for reinforcement behaviors.

Indeed, VTA glutamate neurons have also been implicated in mediating aversive motivation, and it has been difficult to reconcile how mice will perform an instrumental action for optogenetic stimulation of VTA glutamate neurons in one assay while simultaneously showing avoidance behavior in a different assay. For example, mice will avoid an arena paired with optogenetic stimulation of VTA glutamate neurons in a real-time place procedure (RTPP) assay.<sup>10,12,13</sup> Consistent with this, mice will work to turn off stimulation in a negative reinforcement assay.<sup>14</sup> We have previously suggested that the avoidance behavior may be a secondary consequence of the subjects' preference for brief trains of optogenetic stimulation (<5 s) and that this feature distinguishes reinforcement driven by global populations of VTA glutamate versus dopamine neurons.<sup>10</sup> However, another possibility is that glutamate and dopamine released from VTA glutamate projections to NAc shell mediate opposing effects. Indeed, increasing evidence suggests that dopamine release in select NAc sub-regions

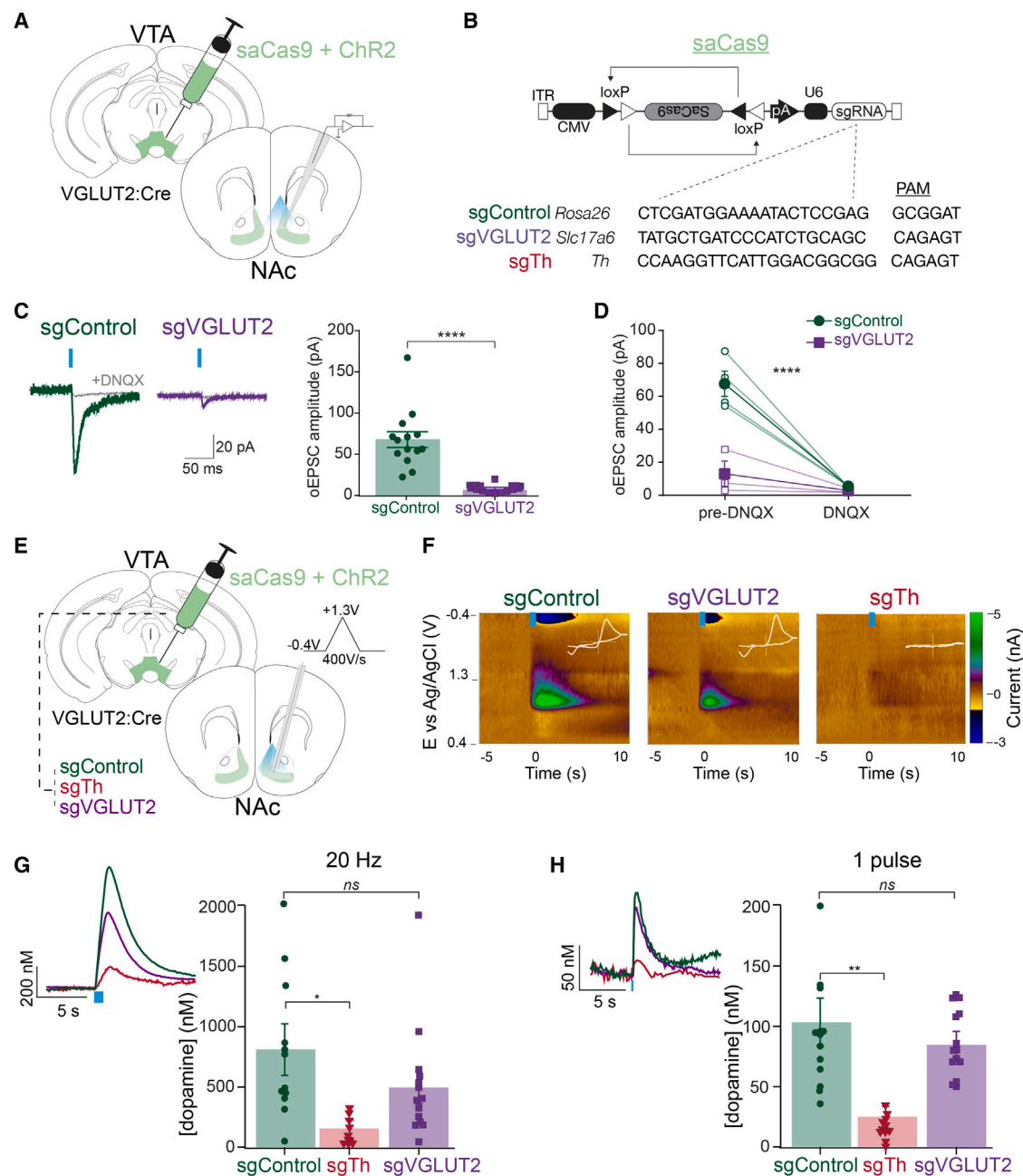


**Figure 1. CRISPR-Cas9 deletion of VGLUT2 or Th in VTA glutamate neurons selectively abolishes glutamate or dopamine co-release**

(A) An illustration of viral injection into the VTA and of the recording patch pipette in postsynaptic NAc neurons.

(B) Design of AAV1-FLEX-SaCas9-U6-sgROSA26 (control), -sgVGLUT2, -sgTh, and with single-guide sequences plus their associated protospacer adjacent motif (PAM) sites.

(C) Example traces of excitatory postsynaptic currents evoked by a 5-ms pulse of optogenetic stimulation (oEPSC) at  $V_h = 70$  mV. oEPSC amplitudes were dramatically reduced in cells from sgVGLUT2 mice ( $n = 14$  sgVGLUT2,  $n = 14$  sgControl; unpaired t test:  $p < 0.0001$ ).

(D) oEPSCs were blocked by bath-application of DNQX ( $n = 7$ ; main effect of treatment:  $p < 0.0001$ ).

(E) Illustration of viral injections into the VTA and carbon fiber electrode recordings in the medial NAc shell applying a triangular waveform from  $-0.4$  to  $1.3$  V at a rate of  $400$  V/s.

(F) Example color plots of phasic dopamine transients in response to optogenetic stimulation ( $20$  Hz,  $1$  s). White insets depict cyclic voltammograms (x axis:  $-0.4$  to  $1.3$  V, y axis:  $-2$  to  $3$  nA).

(legend continued on next page)

relates to aversion.<sup>15–19</sup> Furthermore, recordings from subpopulations of VTA glutamate neurons reveal differential sensitivity to aversive or rewarding stimuli depending on their expression of other neurotransmitter markers, such as for GABA,<sup>20</sup> supporting the notion that subpopulations of VTA glutamate neurons may drive opposing motivations dependent on their expression of a co-transmitter.

In the present study, we tested how glutamate or dopamine release from VTA glutamate terminals in NAc contributes to instrumental reinforcement and place avoidance behaviors evoked by optogenetic stimulation. We show that selective disruption of glutamate release from VTA glutamate neurons via CRISPR-Cas9 abolished optogenetic self-stimulation, but that place avoidance behavior persisted. Conversely, disruption of dopamine release from VTA glutamate neurons abolished optogenetic-evoked place avoidance, whereas self-stimulation remained intact. Finally, disruption of both glutamate and dopamine release from VTA glutamate projections abolished both positive reinforcement and avoidance behaviors. Our results suggest that mesoaccumbens glutamate release is a potent reinforcer but that dopamine co-release from VTA glutamate neurons is aversive.

## RESULTS

### VTA dopamine/glutamate neurons respond to rewarding and aversive stimuli

Prior works show that the global population of VTA glutamate neurons respond to both rewarding and aversive stimuli, although with considerable heterogeneity.<sup>21–24</sup> To specifically test how VTA neurons that co-release both dopamine and glutamate respond to motivationally relevant stimuli, we used fiber photometry. We expressed GCaMP6f in the subset of VTA glutamate neurons that also express a dopamine marker, or, for reference, the global population of VTA glutamate neurons (Figure S1A). We then measured activity in these two populations while presenting mice with a series of motivationally relevant stimuli of either positive or negative valence. We observed that VTA glutamate neurons, including the subpopulation of neurons that release both dopamine and glutamate, are activated during the approach to and consumption of sucrose reward (Figures S1B–S1E). Both populations are also activated during retreat from a threatening looming stimulus or delivery of an aversive footshock (Figures S1F and S1G).

These results suggest that VTA glutamate neurons, including those that co-release dopamine, respond to motivationally relevant stimuli of both positive and negative valence. However, from this approach, it is unclear the extent to which dopamine or glutamate release contributes to these behaviors. Thus, we developed a loss-of-function approach to disambiguate the respective roles of these transmitters to support either positive

reinforcement or avoidance behavior driven by VTA glutamate neuron activity.

### CRISPR-Cas9 disruption of glutamate or dopamine transmission from mesoaccumbens projections

To disrupt glutamate or dopamine release from VTA glutamate neurons, we used a single adeno-associated virus (AAV) vector for Cre recombinase-dependent expression of *Staphylococcus aureus* Cas9 (SaCas9) plus a single-guide RNA (sgRNA) targeted to either the gene encoding VGLUT2 (*Slc17a6*) or tyrosine hydroxylase (*Th*), the rate-limiting enzyme in dopamine biosynthesis.<sup>12,25</sup> When injected into VTA of VGLUT2-Cre mice, Cas9 is expressed selectively in glutamate neurons to generate indel mutations resulting in the loss of either VGLUT2 or TH (among the subset of glutamate neurons that co-release dopamine). To measure the extent to which these manipulations disrupted glutamate or dopamine release, we co-injected AAV to achieve Cre-dependent channelrhodopsin-2 (ChR2) expression, in combination with SaCas9 AAV targeted to either VGLUT2 (sgVGLUT2), TH (sgTh), or a control vector targeted to the Rosa26 locus that is without functional consequence (sgControl) (Figures 1A and 1B). Control experiments demonstrate that these AAV-based manipulations have little effect on the intrinsic membrane properties of VTA glutamate neurons (Figures S2A–S2G) or overall VTA dopamine neuron survival (Figures S2H and S2I).

We first tested the extent to which sgVGLUT2 disrupted glutamate release from VTA terminals in the NAc. After 6 weeks, we recorded optogenetic-evoked excitatory postsynaptic currents (oEPSCs) from medium spiny neurons in the NAc medial shell, where VTA glutamate neurons send dense projections. Cas9 disruption of VTA VGLUT2 significantly reduced the amplitude of oEPSCs compared with sgControl mice; oEPSCs were  $68 \pm 9$  pA in sgControl mice, whereas sgVGLUT2 oEPSCs were  $9 \pm 1$  pA ( $t_{26} = 6.2$ ,  $p < 0.0001$ ), which were 6,7-dinitroquinoxaline-2,3-dione (DNQX)-sensitive ( $F_{1,10} = 42.0$ ,  $p < 0.0001$ ) (Figures 1C and 1D), indicating that CRISPR-Cas9-mediated disruption of VGLUT2 dramatically reduced glutamate release from VTA terminals in the medial NAc shell.

We next used fast-scan cyclic voltammetry (FSCV) to measure optogenetic-evoked dopamine release in the NAc medial shell, comparing sgVGLUT2, sgTh, and sgControl. Both 20-Hz train (473 nm, 1-s duration) and single-pulse (5 ms) stimulation triggered similar levels of dopamine release from VTA glutamate terminals in the NAc medial shell in sgControl and sgVGLUT2 conditions, but the evoked dopamine release was greatly reduced in sgTh mice (Figures 1E–1H). Opto-evoked dopamine transients were not dependent on acetylcholine release secondary to the recruitment of cholinergic interneurons<sup>26–28</sup> because dopamine transients were unaffected by the nicotinic receptor antagonist dihydro- $\beta$ -erythroidine hydrobromide (Dh $\beta$ E) (Figures S2J–S2O).

(G) Peak concentration of dopamine in response to 1 s, 20 Hz stimulation frequency was similar between sgControl ( $n = 12$  slices/4 mice) and sgVGLUT2 ( $n = 14$  slices/5 mice) (Dunnett's multiple comparisons test:  $q = 1.5$ ,  $p > 0.05$ ), but significantly reduced by sgTh ( $n = 11$  slices/4 mice) (Dunnett's multiple comparisons test:  $q = 2.9$ ,  $p < 0.05$ ).

(H) Peak concentration of dopamine in response to a single pulse (5 ms) was similar between sgControl ( $n = 12$  slices/4 mice) and sgVGLUT2 ( $n = 14$  slices/5 mice) (Dunnett's multiple comparisons test:  $q = 1.03$ ,  $p > 0.05$ ), but greatly reduced by sgTh ( $n = 11$  slices/4 mice) (Dunnett's multiple comparisons test:  $q = 3.8$ ,  $p < 0.01$ ). Data are represented as mean  $\pm$  SEM. \* $p < 0.05$ , \*\* $p < 0.01$ , \*\*\*\* $p < 0.0001$ . See also Figure S2.



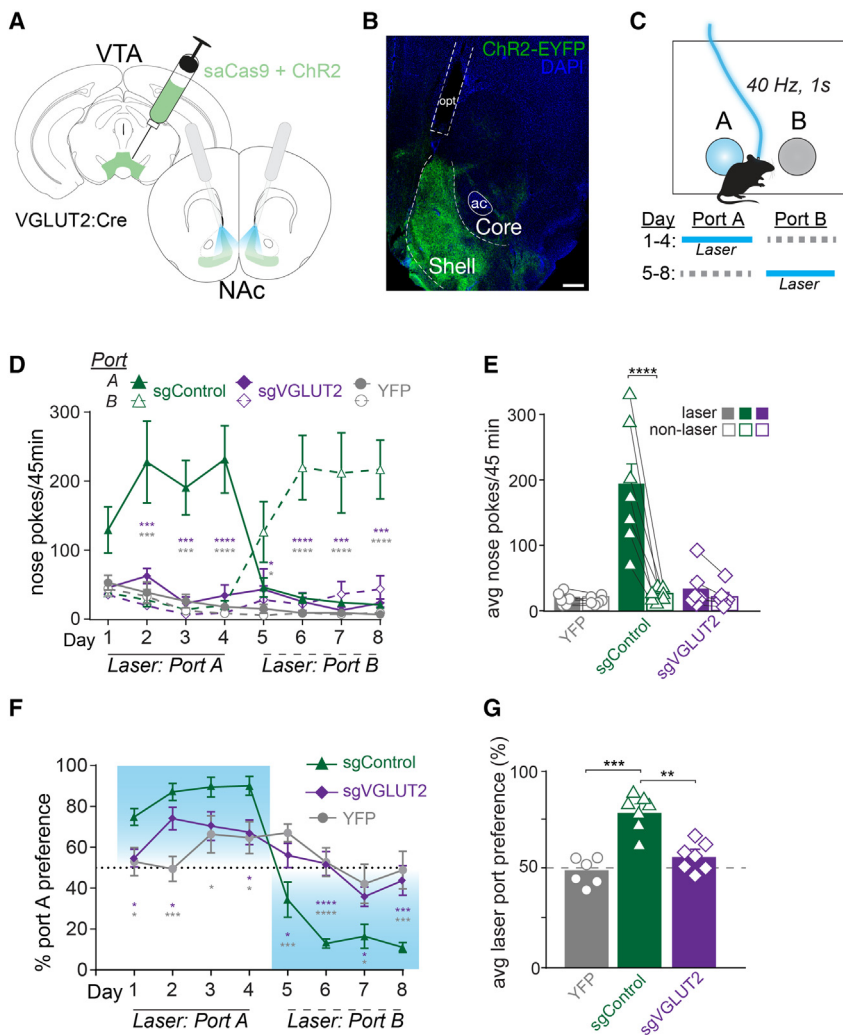


**Figure 2. VTA glutamate projections require glutamate release to promote intracranial self-stimulation**

(A) An illustration of injection into the VTA and optogenetic stimulation of VTA terminals in the NAc with bilateral fiber implants.

(B) An image of the coronal section showing ChR2 (ChR2-EYFP, green) and DAPI (blue) expression in the NAc. Scale bars, 200  $\mu$ m, anterior commissure (ac), optic fiber track (opt).

(C) A schematic of 2-nose-poke intracranial self-stimulation assay. Active nose pokes into the laser-paired port earned 40 Hz, 1 s, 10 mW blue light. The location of the laser-paired port was reversed starting day 5.

(D) The active nose pokes at port A and B during each 45-min session. Sidak's multiple comparisons tests comparing laser-paired pokes between sgControl ( $n = 7$ ) and sgVGLUT2 ( $n = 7$ ; purple asterisks) or between sgControl and YFP ( $n = 6$ ; gray asterisks).

(E) The laser and non-laser nose pokes averaged across all training days. Average laser nose pokes were greater than non-laser nose pokes only among sgControl mice ( $n = 7$ ; Bonferroni multiple comparisons test,  $t = 7.1$ ,  $p < 0.0001$ ).

(F) The percent preference for port A during each training session. Holm-Sidak's multiple comparisons tests comparing laser-paired pokes between sgControl ( $n = 7$ ) and sgVGLUT2 ( $n = 7$ ; purple asterisks) or between sgControl and YFP ( $n = 6$ ; gray asterisks).

(G) The percent of laser port preference averaged across all training days. Average laser port preference among sgControl mice ( $n = 7$ ) was greater than sgVGLUT2 ( $n = 7$ ; Tukey's multiple comparison test,  $q = 7.6$ ,  $p < 0.001$ ) and YFP ( $n = 6$ ; Tukey's multiple comparison test,  $q = 9.5$ ,  $p < 0.0001$ ) groups. Data are represented as mean  $\pm$  SEM. \* $p < 0.05$ , \*\* $p < 0.01$ , \*\*\* $p < 0.001$ , \*\*\*\* $p < 0.0001$ . See also Figure S3.

These results establish that Cas9 disruption of VGLUT2 or TH, respectively, greatly reduces glutamate or dopamine release from VTA glutamate terminals in NAc.

### Mesoaccumbens glutamate release mediates positive reinforcement

Previous work demonstrated that mice nose poke to earn optogenetic stimulation of VTA glutamate neurons, including cell bodies in VTA and their projections to NAc.<sup>10–12</sup> However, there is no direct evidence that it is the glutamate signal that is responsible for this behavioral reinforcement, and one report suggests that mesoaccumbens glutamate release activates NAc interneurons to promote aversion.<sup>14</sup> To assess this, we used two separate reinforcement assays, a nose-poke and a place-based assay. Cre-dependent ChR2 was expressed in VTA of VGLUT2-Cre mice in combination with either sgVGLUT2 or sgControl. A third group received sgControl plus a control for the opsin (yellow fluorescent protein [YFP]), and in all groups, optic fibers were placed to activate VTA terminals in NAc (Figures 2A, 2B, S3A, and S3B).

In an intracranial self-stimulation (ICSS) nose-poke assay, each nose poke into the active port earned laser stimulation (40 Hz, 5-ms pulse width, 1-s duration) plus a 1-s auditory tone. Nose pokes into an inactive port during the same session also triggered the auditory tone, but no laser (Figure 2C). ChR2 mice with intact mesoaccumbens glutamate release (sgControl) self-stimulated, making greater active vs. inactive nose pokes (main effect of port:  $F_{1,6} = 15.1$ ,  $p < 0.01$ ; Figure 2D). Starting on day 5, the location of the active and inactive ports was reversed for the remainder of testing, and sgControl mice tracked the laser location from the first day, making significantly more nose pokes for the new active port than the inactive port (main effect of port:  $F_{1,6} = 11.4$ ,  $p < 0.01$ ). By contrast, sgVGLUT2 mice did not self-stimulate laser, such that active nose pokes by sgControl mice were significantly greater compared with both YFP-expressing mice (without ChR2) and sgVGLUT2 mice across all days (main effect of group:  $F_{2,17} = 12.7$ ,  $p < 0.001$ ; Figure 2E). Correspondingly, sgControl mice displayed an ~80% preference for the active vs. inactive port, which was significantly greater than both sgVGLUT2 and YFP

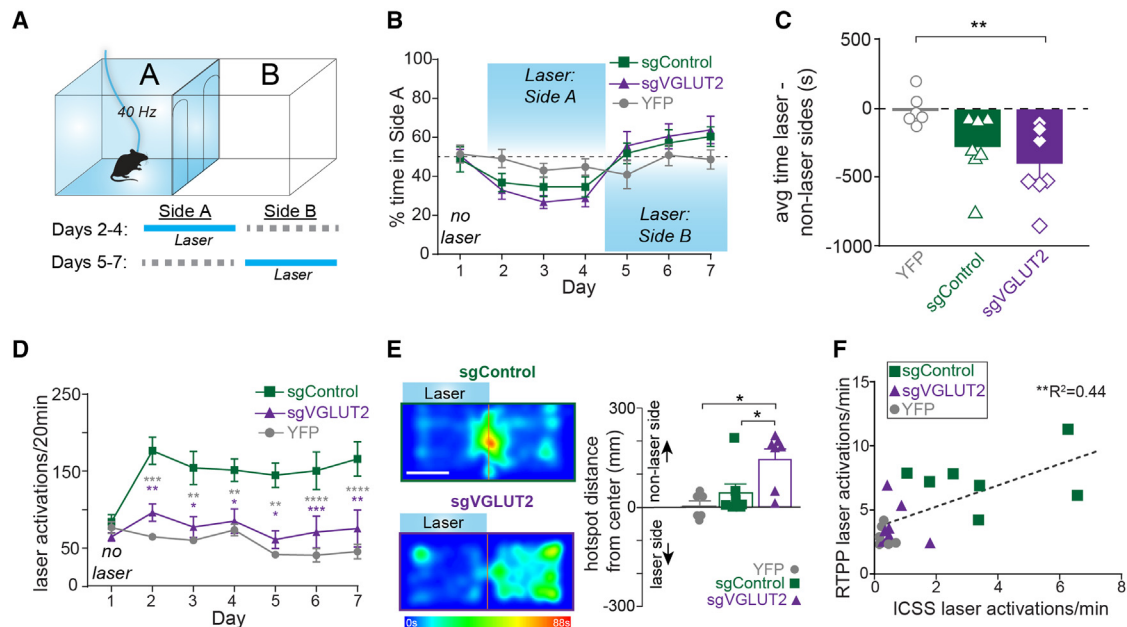


**Figure 3. VTA glutamate projections require glutamate release to promote laser activations but not place avoidance**

(A) A schematic of real-time place procedure (RTPP). Starting on day 2, entries into the laser-paired port earned 40 Hz, 10 mW blue light. The location of the laser-paired side was reversed starting day 5.

(B) The percent time in side A during each 20-min daily session.

(C) The time spent in laser minus non-laser sides averaged across all laser sessions (days 2–7) differed across treatment groups ( $F_2 = 5.4$ ,  $p < 0.05$ ; Dunnett's multiple comparisons: sgVGLUT2 vs. YFP,  $p < 0.01$ ).

(D) The laser activations (identical to number of entries into laser-paired compartment) during each daily 20-min session. The baseline session on day 1 shows entries into compartment, but no laser was delivered. Tukey's multiple comparisons tests comparing laser activations between sgControl ( $n = 7$ ) and sgVGLUT2 ( $n = 7$ ; purple asterisks) or between sgControl and YFP ( $n = 6$ ; gray asterisks).

(E) Example heatmaps from day 4 of RTPP. White scale bars, 135 mm. Bar graph depicts distance from center for each mouse's hotspot (most time spent) on day 4. Hotspots of sgVGLUT2 ( $n = 7$ ) were further away from the center of the compartments than sgControls ( $n = 7$ ; Tukey's multiple comparisons test,  $p < 0.05$ ) and YFPs ( $n = 6$ ; Tukey's multiple comparisons test,  $p < 0.05$ ).

(F) The average laser activations earned per minute across ICSS 2-nose-poke sessions plotted against average laser activations earned per minute across RTPP sessions ( $n = 20$ ; Pearson correlation,  $r = 0.66$ ,  $p < 0.01$ ). Data are represented as mean  $\pm$  SEM. \* $p < 0.05$ , \*\* $p < 0.01$ , \*\*\* $p < 0.001$ . See also Figure S4.

mice (main effect of group:  $F_{2, 17} = 12.2$ ;  $p < 0.001$ ), both of which displayed no preference for active vs. inactive ports (Figures 2F and 2G). These results establish that activation of NAc-projecting VTA glutamate neurons supports positive reinforcement in a manner that depends on VGLUT2-mediated glutamate release.

### Mesoaccumbens glutamate release does not mediate aversion

Previous work has shown that using a RTPP with the delivery of laser stimulation in one of the two compartments, mice spent less time in a compartment paired with activation of mesoaccumbens glutamate neurons.<sup>10,12–14</sup> However, mice simultaneously showed an increase in approach rate, or entries into the laser-paired compartment, and heatmaps depicted a majority of time spent at the intersection between the chambers.<sup>10,12</sup> These data suggest that activation of VTA glutamate neurons may provoke both rewarding and aversive responses, consistent with our observation that VTA dopamine/glutamate neurons respond to both rewarding and aversive stimuli (Figure S1).

Thus, we next used RTPP to assess whether glutamate release by VTA glutamate neurons is necessary for this distinct

signature of positive reinforcement that includes place avoidance but with an increased approach rate. After a baseline day without laser delivery, mice were allowed to trigger laser stimulation by entering one of the two compartments (Figure 3A). On day 4, the laser-paired side was switched for the remainder of the test days. Although YFP-expressing control mice spent similar amounts of time in each compartment, both sgVGLUT2 and sgControl mice spent less time in the laser-paired compartment (side  $\times$  group interaction:  $F_{2, 17} = 3.9$ ,  $p < 0.05$ ). These data indicate that place avoidance evoked by optogenetic stimulation of mesoaccumbens glutamate neurons does not depend on VGLUT2-mediated glutamate release (Figures 3B and 3C).

Although the place avoidance was similar between sgVGLUT2 and sgControl mice, sgVGLUT2 mice failed to show the signature increase in approach rate in this assay. Indeed, we found that the number of laser activations (caused by entry into the laser-paired compartment) increased across sessions in the sgControl mice but did not increase among sgVGLUT2, which was similar to YFP levels (day  $\times$  virus interaction:  $F_{12, 102} = 4.6$ ,  $p < 0.0001$ ; Figure 3D). Furthermore, heatmaps depict that sgControl mice spent a majority of time near the intersection between compartments, presumably as a consequence of their

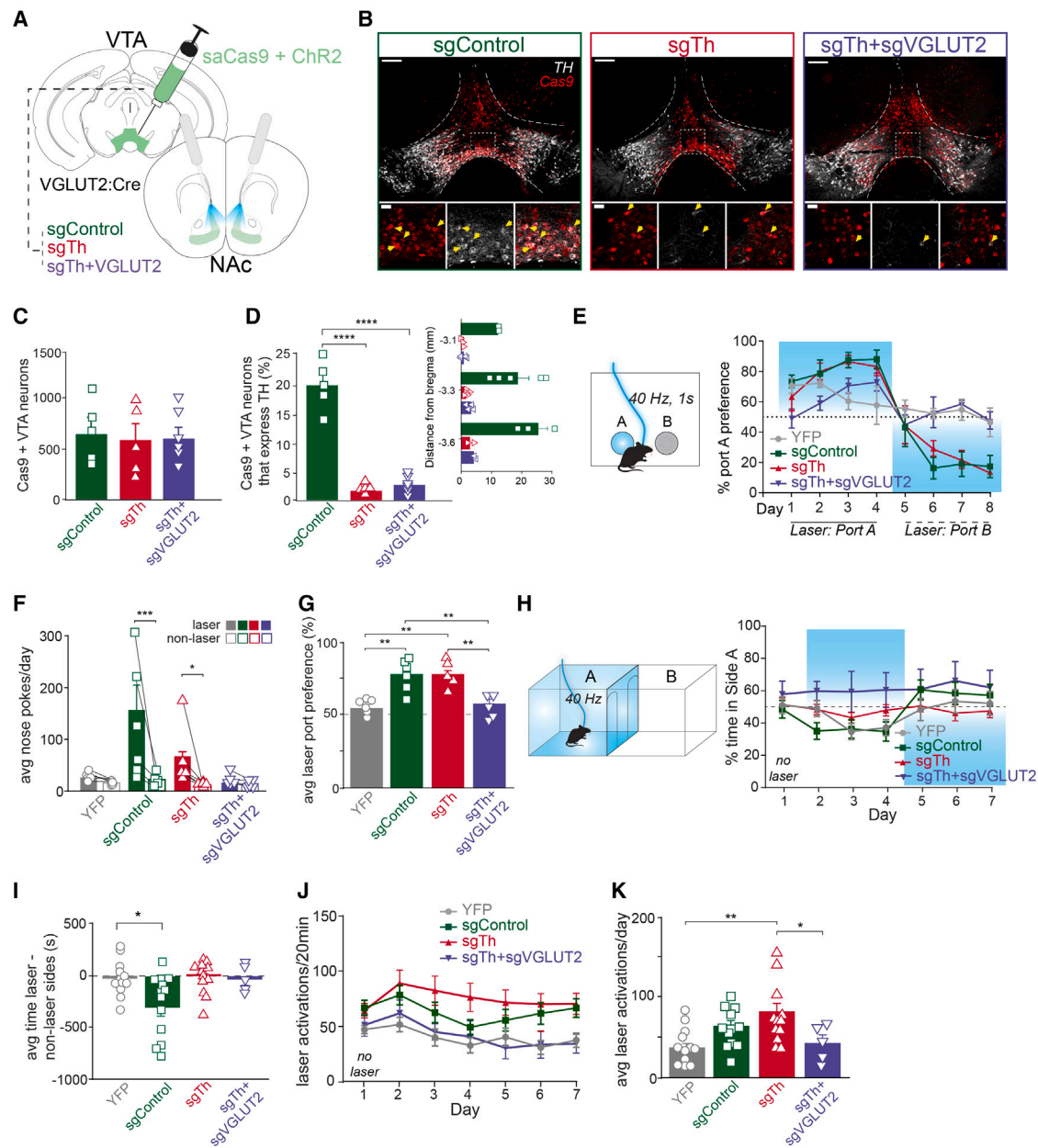


**Figure 4. VTA glutamate projections require dopamine release to promote place avoidance but not self-stimulation**

(A) An illustration of injections in the VTA and optic fiber placements above the NAc.

(B) Images of coronal sections showing Cas9 (red) and TH (white) expressions in the VTA of sgControl, sgTh, and sgTh + sgVGLUT2 mice. Scale bars, 200  $\mu$ m (upper) and 50  $\mu$ m (lower). The yellow arrows indicate cells co-expressing Cas9 and TH.

(C) Amount of Cas9<sup>+</sup> expressing VTA neurons were similar across treatment groups ( $F_{2, 13} = 0.1$ ,  $p > 0.05$ ).

(D) Percent of Cas9 cells in VTA that also express Th was higher in sgControls ( $n = 5$  mice) than sgTh ( $n = 5$  mice; Tukey's multiple comparisons test,  $p < 0.0001$ ) or sgTh + sgVGLUT2 ( $n = 6$  mice; Tukey's multiple comparisons test,  $p < 0.0001$ ). The right inset graph depicts percent Cas9 cells that express TH across anterior to posterior VTA sites.

(E) The schematic of the 2-nose-poke ICSS assay. The percent preference for port A across daily sessions. The location of the laser port was reversed starting on day 5.

(F) The average laser nose pokes were greater than non-laser nose pokes in sgControl mice ( $n = 5$ ; Bonferroni multiple comparisons test,  $p < 0.001$ ) and sgTh mice ( $n = 5$ ;  $p < 0.05$ ).

(G) Holm-Sidak's multiple comparison tests show average laser port preference among sgControl mice ( $n = 5$ ) was greater than YFP ( $n = 6$ ;  $t = 4.3$ ,  $p < 0.01$ ) and sgTh + sgVGLUT2 mice ( $n = 5$ ;  $t = 4.0$ ,  $p < 0.01$ ) but similar to sgTh ( $n = 5$ ;  $t = 0.59$ ,  $p > 0.05$ ), whereas sgTh mice also showed greater laser preference than YFP ( $t = 3.7$ ,  $p < 0.01$ ) and sgTh + sgVGLUT2 mice ( $t = 3.4$ ,  $p < 0.01$ ).

(legend continued on next page)

making frequent brief entries to the laser-paired chamber, whereas sgVGLUT2 subjects spent most of the time in the non-laser-paired compartment further from the center line (distance from the center,  $F_{2, 17} = 6.0$ ,  $p < 0.01$ ; Figure 3E). The failure of sgVGLUT2 mice to show the signature increase in laser compartment entries is unlikely to reflect any baseline motor deficits because the distance traveled in an open-field test was similar between the groups ( $t_{12} = 0.46$ ,  $p > 0.05$ ) (Figure S4A). Instead, the increase in chamber entries made by sgControl mice appears to reflect the seeking of short bouts of laser reinforcement. Consistent with this hypothesis, the number of laser activations received by individual mice in the RTPP is well correlated with the number of laser activations in the nose-poke ICSS assay (Pearson  $r = 0.80$ ,  $p < 0.0001$ ) (Figure 3F).

Optogenetic stimulation of VTA VGLUT2 neurons increased locomotor activity in an open-field arena, consistent with prior reports.<sup>29,30</sup> However, this locomotor increase persisted in sgVGLUT2 mice (Figure S4B), thus failure to locomote is unlikely to account for the absence of stimulation-induced reinforcement in these mice.

Disruption of VTA glutamate release selectively abolished laser self-stimulations in the nose-poke ICSS and RTPP assays, indicating that glutamate release from VTA glutamate neurons mediates positive reinforcement. The lack of positive reinforcement was unlikely due to a generalized deficit in basic reward learning. When tested in an instrumental lever-pressing task to earn food pellets, both sgVGLUT2 and sgControl mice demonstrated similar levels of lever pressing to earn a pellet (main effect of group:  $F_{2, 17} = 0.81$ ,  $p > 0.05$ ) (Figure S4C). Thus, glutamate release from VTA VGLUT2 neurons is responsible for optogenetic reinforcement when these neurons are targeted, but loss of VGLUT2 from these cells does not impair learning a similar instrumental task to obtain a food reinforcer.

### Dopamine co-release from mesoaccumbens glutamate neurons mediates avoidance

Since place avoidance in the RTPP did not depend upon glutamate release from VTA glutamate neurons, we next tested the effects of disrupting dopamine co-release from VTA glutamate neurons on self-stimulation and place avoidance. We expressed Cre-dependent ChR2 in combination with Cre-dependent Sa-Cas9 as follows: (1) targeted to *Th* to disrupt dopamine co-release (sgTh), (2) targeting both *Th* and VGLUT2 to abolish both glutamate and dopamine release (sgTh + sgVGLUT2), (3) targeting the Rosa26 control (sgControl), and (4) a fourth group that expressed YFP instead of ChR2 (Figures 4A, S3C, and S3D). The total number of VTA neurons expressing Cas9 was similar across the treatment groups ( $F_{2, 13} = 0.1$ ,  $p > 0.05$ ), suggesting that we targeted a similar number of cells across the

groups. The fraction of Cas9-expressing VTA neurons that expressed TH was  $20\% \pm 2\%$  in sgControl mice but significantly reduced in mice treated with sgTh ( $2\% \pm 0.3\%$ ) or sgTh + sgVGLUT2 ( $3\% \pm 0.6\%$ ) ( $F_{3, 15} = 33.5$ ,  $p < 0.0001$ ; Figures 4B–4D). These results further validate *Th* disruption by CRISPR-Cas9 and complement our findings that opto-evoked dopamine release from VGLUT2 projections to NAc was blunted in sgTh mice (Figures 1F–1H).

To test the effect of dopamine release from VTA glutamate neurons on positive reinforcement, we first tested mice in the ICSS nose-poke assay. Both sgControl and sgTh mice self-stimulated laser, making more active vs. inactive nose pokes (Figures 4E and 4F). In contrast, both YFP and sgTh + sgVGLUT2 groups made fewer active nose-poke responses and showed no preference for active vs. inactive port (group  $\times$  port interaction:  $F_{3, 18} = 4.5$ ,  $p < 0.05$ ). As a result, sgControl and sgTh mice displayed a high preference for the laser-paired port across training days, compared with equal preference among YFP and sgTh + sgVGLUT2 mice (main effect of group:  $F_{3, 18} = 10.0$ ,  $p < 0.001$ ) (Figure 4G). These results indicate that self-stimulation of VTA glutamate projections to NAc occurs despite abolishing dopamine co-release, consistent with our previous findings,<sup>12</sup> and show that positive reinforcement is abolished when both glutamate and dopamine release are abolished, similar to the effects of disrupting glutamate release alone (Figure 2).

We next tested the contribution of dopamine release by VTA glutamate neurons to place avoidance using the RTPP task (Figure 4H). sgControl mice avoided the laser-paired compartment, spending less time on the laser-paired side than the non-laser side across training days, and switching side preference when the active side was switched on day 5. By contrast, both sgTh and sgTh + sgVGLUT2 mice showed no place avoidance or preference, spending equal time in both compartments without switching preference when the active side was switched (group  $\times$  side interaction:  $F_{3, 18} = 9.1$ ,  $p < 0.01$ ) (Figures 4H and 4I). However, although sgTh mice showed no place avoidance, they continued to show an increased number of entries into the laser side (Figures 4J and 4K). In contrast, the number of laser activations by sgTh + sgVGLUT2 was comparable with YFP opsin controls. Together, these results demonstrate that dopamine co-release from mesoaccumbens glutamate neurons mediates an aversive signal that leads to place avoidance, whereas glutamate release from mesoaccumbens glutamate neurons promotes positive reinforcement.

## DISCUSSION

Stimulation of VTA glutamate neuron projections to the NAc medial shell simultaneously promotes not only positive

(H) The schematic of the RTPP assay. The percent time in side A during each 20-min daily session. No laser was delivered on day 1, and the location of the laser side was reversed on day 5.

(I) The time spent in laser minus non-laser sides averaged across all laser sessions (days 2–7), differed across treatment groups ( $F_3 = 4.8$ ,  $p < 0.01$ ; Dunnett's multiple comparisons: sgControl ( $n = 13$ ) vs. YFP ( $n = 12$ ),  $p < 0.05$ ; sgTh ( $n = 12$ ) vs. YFP,  $p > 0.05$ ; sgTh + sgVGLUT2 ( $n = 6$ ) vs. YFP,  $p > 0.05$ ).

(J) The laser activations earned during each daily 20-min session.

(K) The laser activations averaged across laser sessions in sgTh mice were higher than YFP mice (Tukey's multiple comparisons test,  $p < 0.01$ ) and sgTh + sgVGLUT2 mice (Tukey's multiple comparisons test,  $p < 0.05$ ). Data are represented as mean  $\pm$  SEM. \* $p < 0.05$ , \*\* $p < 0.01$ , \*\*\* $p < 0.001$ , \*\*\*\* $p < 0.0001$ . See also Figure S3.



reinforcement but also place avoidance. Here, we demonstrate that glutamate release by VGLUT2<sup>+</sup> VTA neurons is necessary for stimulation-evoked positive reinforcement, whereas dopamine release from VGLUT2<sup>+</sup> VTA neurons is required for avoidance. Selectively disrupting VGLUT2 from VTA neurons through the CRISPR-Cas9 endonuclease blunted glutamate release without disrupting co-released dopamine. As a result, self-stimulation in both nose-poke and place-based (laser-side entries) assays was abolished. However, VGLUT2 disruption did not alter place avoidance caused by stimulation of VGLUT2<sup>+</sup> VTA neurons. By contrast, selective disruption of dopamine co-release from VTA glutamate neurons left positive reinforcement intact but abolished place avoidance, indicating that dopamine released from VTA glutamate neurons promotes aversion. We further demonstrate that CRISPR-Cas9 deletion of both TH and VGLUT2 completely abolished both self-stimulation and avoidance behaviors. These results demonstrate that glutamate and dopamine released by NAc-projecting VTA glutamate neurons differentially contribute to reward and aversion.

### Mesoaccumbal glutamate release promotes positive reinforcement

Optogenetic activation of excitatory inputs to the NAc from amygdala, hippocampus, and cortex has been repeatedly shown to reinforce behaviors.<sup>31–34</sup> Our results are consistent with those of prior works and support a prominent role for excitatory inputs to NAc from VTA in positive reinforcement.<sup>10–12</sup> Our findings are also consistent with studies showing that conditional disruption of glutamate release from VTA dopamine neurons disrupts psychomotor sensitization and alters reward-seeking behaviors,<sup>30,35–38</sup> that photoinhibition of VTA glutamate neurons disrupts cue-reward associations,<sup>39</sup> and that VTA glutamate neurons are activated by rewards and reward-predictive cues.<sup>20,24</sup>

On the other hand, disrupting glutamate release from dopamine neurons does not blunt optogenetic self-stimulation of dopamine neurons.<sup>40</sup> The most likely explanation for this is that only a minority of VTA dopamine neurons express VGLUT2, and that stimulation of the global population of VTA dopamine neurons is sufficient to support strong positive reinforcement independent of glutamate co-release from a minority subset of dopamine neurons. We have also shown that when comparing the effects of stimulating the global pool of VTA glutamate vs. the global pool of VTA dopamine neurons, mice prefer brief trains of VTA glutamate neuron stimulation (<5 s) but prefer more sustained trains of VTA dopamine neuron stimulation (>5 s).<sup>10</sup> Thus, the release of glutamate from VTA neurons promotes reward-related motivation that is distinct and independent from dopamine.

### Positive reinforcement and avoidance are separable features of VTA glutamate neuron activation

Although stimulation of mesoaccumbal glutamate projections promotes self-stimulation and approach behavior, stimulation of these projections simultaneously results in place avoidance during real-time place assays.<sup>10,12,14</sup> Furthermore, VTA glutamate neurons, including the subpopulation of glutamate neurons that co-release dopamine (Figure S1), increase their intrinsic activity in response to both rewarding and aversive stimuli.<sup>21,23,24</sup>

Together, these data support a role for VTA glutamate neurons not only in reward but also in aversion.

VTA glutamate neurons target diverse cell types in NAc.<sup>41–45</sup> Prior work suggested a role for VTA glutamate neuron activation of NAc parvalbumin (PV)-expressing interneurons in driving aversive behaviors.<sup>14</sup> However, a more recent study showed that direct activation of NAc PV interneurons elicits a conditioned place preference, whereas their inhibition produces conditioned avoidance,<sup>46</sup> suggesting that avoidance is unlikely to be mediated via glutamatergic activation of PV interneurons. Nevertheless, microinjection of dopamine receptor antagonists into NAc did not abolish avoidance behavior induced by the stimulation of VTA glutamate inputs.<sup>14</sup> Although it is difficult to control the functional spread of microinjected agents, this null result may be due to the dorsal site targeted within NAc. Indeed, recent studies have highlighted the role of dopamine in the ventral medial shell of NAc in avoidance behaviors.<sup>15,47</sup> On the other hand, microinjection of glutamate (or GABA) receptor antagonists in NAc blocked place avoidance mediated by VTA glutamate stimulation.<sup>14</sup> However, this approach is not selective to the synapses under investigation and instead blocks all excitatory (or inhibitory) synapses, which may account for the absence of an optogenetic-evoked behavioral effect. Indeed, dopamine's effect on NAc activity is likely to depend crucially on its ability to modulate other excitatory or inhibitory inputs.<sup>48</sup>

Our results propose an alternate explanation for the mixed positively and negatively reinforcing effects observed upon activation of VTA glutamate neurons while also explaining why at least a subset of VTA glutamate neurons (those that co-release dopamine) may be activated by both rewarding and aversive stimuli. We propose not only that, like other glutamatergic inputs to NAc,<sup>31,32,49,50</sup> glutamate released from VTA terminals in NAc is positively reinforcing but also that dopamine, which is co-released from a subset of these cells, leads to an aversive response. We further posit that co-release of recycling neurotransmitters from other populations of neurons within the limbic system may support opposite motivational responses, for example, the co-release of GABA and glutamate from VTA or pallidal inputs to lateral habenula<sup>10,51–54</sup> or the co-release of acetylcholine and glutamate at habenulopeduncular synapses.<sup>55,56</sup>

### VTA glutamate projections require dopamine co-release to promote avoidance

Although dopamine is best known for supporting reward-related motivation, growing evidence points to diverse roles for dopamine across heterogeneous striatal sub-regions and cell types.<sup>17,47</sup> Specifically, it has been repeatedly established that some dopamine neurons are activated in response to aversive stimuli.<sup>57–59</sup> In particular, the medial NAc shell, which receives the densest fraction of glutamatergic fibers from VTA,<sup>60,61</sup> is an apparent hotspot for dopamine release evoked by aversive stimuli. For example, multiple studies reported dopamine release in the medial NAc shell in response to an aversive or stressful stimulus (e.g., foot shock or threatening odor) or its associated cue; this is in contrast to lateral NAc or NAc core, where dopamine release decreased in response to aversive stimuli.<sup>15,16,18,19</sup> Mesolimbic dopamine is also critical for aversive processes such as innate defensive behaviors and fear conditioning,<sup>62–65</sup> and one

recent study showed a role for VTA glutamate neurons in mediating defensive responses to a looming threat.<sup>29</sup>

Our present findings demonstrate that mesolimbic dopamine, specifically co-released by VGLUT2-expressing VTA glutamate neurons, induces avoidance behavior elicited by the optogenetic activation of these neurons. Thus, the source of dopamine evoked in response to aversive stimuli is likely to include dopamine neurons that also release glutamate. Whether dopamine release from non-glutamate dopamine neurons that project to the medial NAc shell also contributes to aversive responses remains unknown. It is similarly unknown whether glutamate/dopamine and glutamate/non-dopamine mesoaccumbens neurons have similar or distinct roles in approach or avoidance behaviors. For example, one estimate suggests that ~23% of the VGLUT2<sup>+</sup> neurons projecting to NAc are TH negative.<sup>8</sup> We presume that these VGLUT2<sup>+</sup>/TH<sup>−</sup> neurons contribute to the behavioral outcomes we measured, and it remains plausible that glutamate release from VGLUT2<sup>+</sup>/TH<sup>+</sup> vs. VGLUT2<sup>+</sup>/TH<sup>−</sup> neurons would differentially contribute to reward or aversion. Future experiments employing multi-recombinase intersectional approaches to manipulate these subpopulations may shine light on these unknowns.

## Conclusions

Our data demonstrate that VTA glutamate projections promote positive reinforcement through the release of glutamate and simultaneously promote avoidance that instead relies on the co-release of dopamine. This evidence further highlights mesolimbic contributions to reinforcement that are dopamine-independent and expands our understanding of neurotransmitter-specific roles within co-releasing populations. Our findings also add to the growing evidence implicating opposing reward and aversion functions of mesolimbic dopamine signals and the importance of studying the role of dopamine and non-dopamine VTA sub-types. Indeed, the ability of a neuronal population to promote divergent functions at the level of their multiple neurotransmitters has complex implications for understanding disorders involving dysregulated reward or aversion, including substance use or compulsive disorders.

## STAR★METHODS

Detailed methods are provided in the online version of this paper and include the following:

- **KEY RESOURCES TABLE**
- **RESOURCE AVAILABILITY**
  - Lead contact
  - Materials availability
  - Data and code availability
- **EXPERIMENTAL MODEL AND STUDY PARTICIPANT DETAILS**
- **METHOD DETAILS**
  - Viral production
  - Stereotactic surgeries
  - Immunohistochemistry
  - Electrophysiological recordings in mouse brain slices
  - *In vitro* fast-scan cyclic voltammetry recordings

- Fiber photometry recordings
- 2 nose-poke optogenetic self-stimulation procedure
- Real-time place preference/avoidance procedure
- Open Field

## ● QUANTIFICATION AND STATISTICAL ANALYSIS

## SUPPLEMENTAL INFORMATION

Supplemental information can be found online at <https://doi.org/10.1016/j.neuron.2023.11.002>.

## ACKNOWLEDGMENTS

This work was supported by grants from NIH (R01DA036612, F32MH122192, P30DA048736, and K99MH130688) and Veterans Affairs (I01BX005782).

## AUTHOR CONTRIBUTIONS

Conceptualization, S.M.W. and T.S.H.; methodology, S.M.W., S.M.S., V.Z., and T.S.H.; investigation, S.M.W., S.M.S., N.G.H., and D.S.D.; formal analysis, S.M.W., S.M.S., L.F., and T.S.H.; writing – original draft, S.M.W. and T.S.H.; writing – review and editing, S.M.W., S.M.S., L.S.Z., and T.S.H.; resources, A.C.H. and L.S.Z.; funding acquisition, S.M.W. and T.S.H.

## DECLARATION OF INTERESTS

The authors declare no competing interests.

Received: March 21, 2022

Revised: June 22, 2023

Accepted: November 6, 2023

Published: December 11, 2023

## REFERENCES

1. Pupe, S., and Wallén-Mackenzie, Å. (2015). Cre-driven optogenetics in the heterogeneous genetic panorama of the VTA. *Trends Neurosci.* 38, 375–386. <https://doi.org/10.1016/j.tins.2015.04.005>.
2. Trudeau, L.-E., Hnasko, T.S., Wallén-Mackenzie, A., Morales, M., Rayport, S., and Sulzer, D. (2014). The multilingual nature of dopamine neurons. *Prog. Brain Res.* 211, 141–164. <https://doi.org/10.1016/B978-0-444-63425-2.00006-4>.
3. Hnasko, T.S., and Edwards, R.H. (2012). Neurotransmitter corelease: mechanism and physiological role. *Annu. Rev. Physiol.* 74, 225–243. <https://doi.org/10.1146/annurev-physiol-020911-153315>.
4. Eskenazi, D., Malave, L., Mingote, S., Yetnikoff, L., Ztaou, S., Velicu, V., Rayport, S., and Chuhma, N. (2021). Dopamine neurons that cotransmit glutamate, from synapses to circuits to behavior. *Front. Neural Circuits* 15, 665386. <https://doi.org/10.3389/fncir.2021.665386>.
5. Kawano, M., Kawasaki, A., Sakata-Haga, H., Fukui, Y., Kawano, H., Nogami, H., and Hisano, S. (2006). Particular subpopulations of midbrain and hypothalamic dopamine neurons express vesicular glutamate transporter 2 in the rat brain. *J. Comp. Neurol.* 498, 581–592. <https://doi.org/10.1002/cne.21054>.
6. Stuber, G.D., Hnasko, T.S., Britt, J.P., Edwards, R.H., and Bonci, A. (2010). Dopaminergic terminals in the nucleus accumbens but not the dorsal striatum corelease glutamate. *J. Neurosci.* 30, 8229–8233. <https://doi.org/10.1523/JNEUROSCI.1754-10.2010>.
7. Tecuapetla, F., Patel, J.C., Xenias, H., English, D., Tadros, I., Shah, F., Berlin, J., Deisseroth, K., Rice, M.E., Tepper, J.M., et al. (2010). Glutamatergic signaling by mesolimbic dopamine neurons in the nucleus accumbens. *J. Neurosci.* 30, 7105–7110. <https://doi.org/10.1523/JNEUROSCI.0265-10.2010>.

8. Yamaguchi, T., Wang, H.-L., Li, X., Ng, T.H., and Morales, M. (2011). Mesocorticolimbic glutamatergic pathway. *J. Neurosci.* 31, 8476–8490. <https://doi.org/10.1523/JNEUROSCI.1598-11.2011>.
9. Chuhma, N., Zhang, H., Masson, J., Zhuang, X., Sulzer, D., Hen, R., and Rayport, S. (2004). Dopamine neurons mediate a fast excitatory signal via their glutamatergic synapses. *J. Neurosci.* 24, 972–981. <https://doi.org/10.1523/JNEUROSCI.4317-03.2004>.
10. Yoo, J.H., Zell, V., Gutierrez-Reed, N., Wu, J., Ressler, R., Shenasa, M.A., Johnson, A.B., Fife, K.H., Faget, L., and Hnasko, T.S. (2016). Ventral tegmental area glutamate neurons co-release GABA and promote positive reinforcement. *Nat. Commun.* 7, 13697. <https://doi.org/10.1038/ncomms13697>.
11. Wang, H.-L., Qi, J., Zhang, S., Wang, H., and Morales, M. (2015). Rewarding effects of optical stimulation of ventral tegmental area glutamatergic neurons. *J. Neurosci.* 35, 15948–15954. <https://doi.org/10.1523/JNEUROSCI.3428-15.2015>.
12. Zell, V., Steinkellner, T., Hollon, N.G., Warlow, S.M., Souter, E., Faget, L., Hunker, A.C., Jin, X., Zweifel, L.S., and Hnasko, T.S. (2020). VTA glutamate neuron activity drives positive reinforcement absent dopamine co-release. *Neuron* 107, 864–873.e4. <https://doi.org/10.1016/j.neuron.2020.06.011>.
13. Bimpisidis, Z., König, N., Stagkourakis, S., Zell, V., Vlcek, B., Dumas, S., Giros, B., Broberger, C., Hnasko, T.S., and Wallén-Mackenzie, Å. (2019). The neurod6 subtype of VTA neurons contributes to psychostimulant sensitization and behavioral reinforcement. *eNeuro* 6, ENEURO.0066-19.2019. <https://doi.org/10.1523/ENEURO.0066-19.2019>.
14. Qi, J., Zhang, S., Wang, H.-L., Barker, D.J., Miranda-Barrientos, J., and Morales, M. (2016). VTA glutamatergic inputs to nucleus accumbens drive aversion by acting on GABAergic interneurons. *Nat. Neurosci.* 19, 725–733. <https://doi.org/10.1038/nn.4281>.
15. de Jong, J.W., Afjei, S.A., Pollak Dorocic, I., Peck, J.R., Liu, C., Kim, C.K., Tian, L., Deisseroth, K., and Lammel, S. (2019). A neural circuit mechanism for encoding aversive stimuli in the mesolimbic dopamine system. *Neuron* 101, 133–151.e7. <https://doi.org/10.1016/j.neuron.2018.11.005>.
16. Badrinarayan, A., Wescott, S.A., Vander Weele, C.M., Saunders, B.T., Couturier, B.E., Maren, S., and Aragona, B.J. (2012). Aversive stimuli differentially modulate real-time dopamine transmission dynamics within the nucleus accumbens core and shell. *J. Neurosci.* 32, 15779–15790. <https://doi.org/10.1523/JNEUROSCI.3557-12.2012>.
17. Wenzel, J.M., Rauscher, N.A., Cheer, J.F., and Oleson, E.B. (2015). A role for phasic dopamine release within the nucleus accumbens in encoding aversion: a review of the neurochemical literature. *ACS Chem. Neurosci.* 6, 16–26. <https://doi.org/10.1021/cn500255p>.
18. Yuan, L., Dou, Y.-N., and Sun, Y.-G. (2019). Topography of reward and aversion encoding in the mesolimbic dopaminergic system. *J. Neurosci.* 39, 6472–6481. <https://doi.org/10.1523/JNEUROSCI.0271-19.2019>.
19. Deutch, A.Y., and Cameron, D.S. (1992). Pharmacological characterization of dopamine systems in the nucleus accumbens core and shell. *Neuroscience* 46, 49–56. [https://doi.org/10.1016/0306-4522\(92\)90007-o](https://doi.org/10.1016/0306-4522(92)90007-o).
20. Root, D.H., Barker, D.J., Estrin, D.J., Miranda-Barrientos, J.A., Liu, B., Zhang, S., Wang, H.-L., Vautier, F., Ramakrishnan, C., Kim, Y.S., et al. (2020). Distinct signaling by ventral tegmental area glutamate, GABA, and combinatorial glutamate-GABA neurons in motivated behavior. *Cell Rep.* 32, 108094. <https://doi.org/10.1016/j.celrep.2020.108094>.
21. Montardy, Q., Zhou, Z., Lei, Z., Liu, X., Zeng, P., Chen, C., Liu, Y., Sanz-Leon, P., Huang, K., and Wang, L. (2019). Characterization of glutamatergic VTA neural population responses to aversive and rewarding conditioning in freely-moving mice. *Sci. Bull.* 64, 1167–1178. <https://doi.org/10.1016/j.scib.2019.05.005>.
22. McGovern, D.J., Ly, A., Ecton, K.L., Huynh, D.T., Prévost, E.D., Gonzalez, S.C., McNulty, C.J., Rau, A.R., Hentges, S.T., Daigle, T.L., et al. (2022). Ventral tegmental area glutamate neurons mediate nonassociative consequences of stress. *Mol. Psychiatry*. <https://doi.org/10.1038/s41380-022-01858-3>.
23. Root, D.H., Estrin, D.J., and Morales, M. (2018). Aversion or salience signaling by ventral tegmental area glutamate neurons. *iScience* 2, 51–62. <https://doi.org/10.1016/j.isci.2018.03.008>.
24. McGovern, D.J., Polter, A.M., and Root, D.H. (2021). Neurochemical signaling of reward and aversion to ventral tegmental area glutamate neurons. *J. Neurosci.* 41, 5471–5486. <https://doi.org/10.1523/JNEUROSCI.1419-20.2021>.
25. Hunker, A.C., Soden, M.E., Krayushkina, D., Heymann, G., Awatramani, R., and Zweifel, L.S. (2020). Conditional single vector crispr/sacas9 viruses for efficient mutagenesis in the adult mouse nervous system. *Cell Rep.* 30, 4303–4316.e6. <https://doi.org/10.1016/j.celrep.2020.02.092>.
26. Threlfell, S., Lalic, T., Platt, N.J., Jennings, K.A., Deisseroth, K., and Cragg, S.J. (2012). Striatal dopamine release is triggered by synchronized activity in cholinergic interneurons. *Neuron* 75, 58–64. <https://doi.org/10.1016/j.neuron.2012.04.038>.
27. Cachope, R., Mateo, Y., Mathur, B.N., Irving, J., Wang, H.-L., Morales, M., Lovinger, D.M., and Cheer, J.F. (2012). Selective activation of cholinergic interneurons enhances accumbal phasic dopamine release: setting the tone for reward processing. *Cell Rep.* 2, 33–41. <https://doi.org/10.1016/j.celrep.2012.05.011>.
28. Shin, J.H., Adrover, M.F., Wess, J., and Alvarez, V.A. (2015). Muscarinic regulation of dopamine and glutamate transmission in the nucleus accumbens. *Proc. Natl. Acad. Sci. USA* 112, 8124–8129. <https://doi.org/10.1073/pnas.1508846112>.
29. Barbano, M.F., Wang, H.-L., Zhang, S., Miranda-Barrientos, J., Estrin, D.J., Figueroa-González, A., Liu, B., Barker, D.J., and Morales, M. (2020). VTA glutamatergic neurons mediate innate defensive behaviors. *Neuron* 107, 368–382.e8. <https://doi.org/10.1016/j.neuron.2020.04.024>.
30. Birgner, C., Nordenankar, K., Lundblad, M., Mendez, J.A., Smith, C., le Grevès, M., Galter, D., Olson, L., Fredriksson, A., Trudeau, L.-E., et al. (2010). VGLUT2 in dopamine neurons is required for psychostimulant-induced behavioral activation. *Proc. Natl. Acad. Sci. USA* 107, 389–394. <https://doi.org/10.1073/pnas.0910986107>.
31. Britt, J.P., Benaliouad, F., McDevitt, R.A., Stuber, G.D., Wise, R.A., and Bonci, A. (2012). Synaptic and behavioral profile of multiple glutamatergic inputs to the nucleus accumbens. *Neuron* 76, 790–803. <https://doi.org/10.1016/j.neuron.2012.09.040>.
32. Stuber, G.D., Sparta, D.R., Stamatakis, A.M., van Leeuwen, W.A., Hardjoprajitno, J.E., Cho, S., Tye, K.M., Kempadoo, K.A., Zhang, F., Deisseroth, K., et al. (2011). Excitatory transmission from the amygdala to nucleus accumbens facilitates reward seeking. *Nature* 475, 377–380. <https://doi.org/10.1038/nature10194>.
33. LeGates, T.A., Kvarta, M.D., Tooley, J.R., Francis, T.C., Lobo, M.K., Creed, M.C., and Thompson, S.M. (2018). Reward behaviour is regulated by the strength of hippocampus-nucleus accumbens synapses. *Nature* 564, 258–262. <https://doi.org/10.1038/s41586-018-0740-8>.
34. Otis, J.M., Namboodiri, V.M.K., Matan, A.M., Voets, E.S., Mohorn, E.P., Kosyk, O., McHenry, J.A., Robinson, J.E., Resendez, S.L., Rossi, M.A., et al. (2017). Prefrontal cortex output circuits guide reward seeking through divergent cue encoding. *Nature* 543, 103–107. <https://doi.org/10.1038/nature21376>.
35. Papanthou, M., Creed, M., Dorst, M.C., Bimpisidis, Z., Dumas, S., Pettersson, H., Bellone, C., Silberberg, G., Lüscher, C., and Wallén-Mackenzie, Å. (2018). Targeting VGLUT2 in mature dopamine neurons decreases mesoaccumbal glutamatergic transmission and identifies a role for glutamate co-release in synaptic plasticity by increasing baseline AMPA/NMDA ratio. *Front. Neural Circuits* 12, 64. <https://doi.org/10.3389/fncir.2018.00064>.
36. Alsö, J., Nordenankar, K., Arvidsson, E., Birgner, C., Mahmoudi, S., Halbout, B., Smith, C., Fortin, G.M., Olson, L., Descarries, L., et al. (2011). Enhanced sucrose and cocaine self-administration and cue-induced drug seeking after loss of VGLUT2 in midbrain dopamine neurons in mice. *J. Neurosci.* 31, 12593–12603. <https://doi.org/10.1523/JNEUROSCI.2397-11.2011>.

37. Hnasko, T.S., Chuhma, N., Zhang, H., Goh, G.Y., Sulzer, D., Palmiter, R.D., Rayport, S., and Edwards, R.H. (2010). Vesicular glutamate transport promotes dopamine storage and glutamate corelease in vivo. *Neuron* 65, 643–656. <https://doi.org/10.1016/j.neuron.2010.02.012>.
38. Mingote, S., Chuhma, N., Kalmbach, A., Thomsen, G.M., Wang, Y., Mihali, A., Sferazza, C., Zucker-Scharff, I., Siena, A.-C., Welch, M.G., et al. (2017). Dopamine neuron dependent behaviors mediated by glutamate cotransmission. *eLife* 6, e27566. <https://doi.org/10.7554/eLife.27566>.
39. Yau, H.-J., Wang, D.V., Tsou, J.-H., Chuang, Y.-F., Chen, B.T., Deisseroth, K., Ikemoto, S., and Bonci, A. (2016). Pontomesencephalic tegmental afferents to VTA non-dopamine neurons are necessary for appetitive Pavlovian learning. *Cell Rep.* 16, 2699–2710. <https://doi.org/10.1016/j.celrep.2016.08.007>.
40. Wang, D.V., Viereckel, T., Zell, V., Konradsson-Geuken, Å., Broker, C.J., Talishinsky, A., Yoo, J.H., Galinato, M.H., Arvidsson, E., Kesner, A.J., et al. (2017). Disrupting glutamate co-transmission does not affect acquisition of conditioned behavior reinforced by dopamine neuron activation. *Cell Rep.* 18, 2584–2591. <https://doi.org/10.1016/j.celrep.2017.02.062>.
41. Mingote, S., Amsellem, A., Kempf, A., Rayport, S., and Chuhma, N. (2019). Dopamine-glutamate neuron projections to the nucleus accumbens medial shell and behavioral switching. *Neurochem. Int.* 129, 104482. <https://doi.org/10.1016/j.neuint.2019.104482>.
42. Chuhma, N., Mingote, S., Moore, H., and Rayport, S. (2014). Dopamine neurons control striatal cholinergic neurons via regionally heterogeneous dopamine and glutamate signaling. *Neuron* 81, 901–912. <https://doi.org/10.1016/j.neuron.2013.12.027>.
43. Chuhma, N., Oh, S.J., and Rayport, S. (2023). The dopamine neuron synaptic map in the striatum. *Cell Rep.* 42, 112204. <https://doi.org/10.1016/j.celrep.2023.112204>.
44. Mingote, S., Chuhma, N., Kusnoor, S.V., Field, B., Deutch, A.Y., and Rayport, S. (2015). Functional connectome analysis of dopamine neuron glutamatergic connections in forebrain regions. *J. Neurosci.* 35, 16259–16271. <https://doi.org/10.1523/JNEUROSCI.1674-15.2015>.
45. Cai, Y., and Ford, C.P. (2018). Dopamine cells differentially regulate striatal cholinergic transmission across regions through corelease of dopamine and glutamate. *Cell Rep.* 25, 3148–3157.e3. <https://doi.org/10.1016/j.celrep.2018.11.053>.
46. Chen, X., Liu, Z., Ma, C., Ma, L., and Liu, X. (2019). Parvalbumin interneurons determine emotional valence through modulating accumbal output pathways. *Front. Behav. Neurosci.* 13, 110. <https://doi.org/10.3389/fnbeh.2019.00110>.
47. de Jong, J.W., Fraser, K.M., and Lammel, S. (2022). Mesoaccumbal dopamine heterogeneity: what do dopamine firing and release have to do with it? *Annu. Rev. Neurosci.* 45, 109–129. <https://doi.org/10.1146/annurev-neuro-110920-011929>.
48. Nicola, S.M., Surmeier, J., and Malenka, R.C. (2000). Dopaminergic modulation of neuronal excitability in the striatum and nucleus accumbens. *Annu. Rev. Neurosci.* 23, 185–215. <https://doi.org/10.1146/annurev-neuro.23.1.185>.
49. Parker, N.F., Baidya, A., Cox, J., Haetzel, L.M., Zhukovskaya, A., Murugan, M., Engelhard, B., Goldman, M.S., and Witten, I.B. (2022). Choice-selective sequences dominate in cortical relative to thalamic inputs to NAc to support reinforcement learning. *Cell Rep.* 39, 110756. <https://doi.org/10.1016/j.celrep.2022.110756>.
50. Namburi, P., Beyeler, A., Yorozu, S., Calhoon, G.G., Halbert, S.A., Wichmann, R., Holden, S.S., Mertens, K.L., Anahtar, M., Felix-Ortiz, A.C., et al. (2015). A circuit mechanism for differentiating positive and negative associations. *Nature* 520, 675–678. <https://doi.org/10.1038/nature14366>.
51. Root, D.H., Mejias-Aponte, C.A., Qi, J., and Morales, M. (2014). Role of glutamatergic projections from ventral tegmental area to lateral habenula in aversive conditioning. *J. Neurosci.* 34, 13906–13910. <https://doi.org/10.1523/JNEUROSCI.2029-14.2014>.
52. Lammel, S., Steinberg, E.E., Földy, C., Wall, N.R., Beier, K., Luo, L., and Malenka, R.C. (2015). Diversity of transgenic mouse models for selective targeting of midbrain dopamine neurons. *Neuron* 85, 429–438. <https://doi.org/10.1016/j.neuron.2014.12.036>.
53. Shabel, S.J., Proulx, C.D., Piriz, J., and Malinow, R. (2014). Mood regulation. GABA/glutamate co-release controls habenula output and is modified by antidepressant treatment. *Science* 345, 1494–1498. <https://doi.org/10.1126/science.1250469>.
54. Meye, F.J., Soiza-Reilly, M., Smit, T., Diana, M.A., Schwarz, M.K., and Mameli, M. (2016). Shifted pallidal co-release of GABA and glutamate in habenula drives cocaine withdrawal and relapse. *Nat. Neurosci.* 19, 1019–1024. <https://doi.org/10.1038/nn.4334>.
55. Frahm, S., Antolin-Fontes, B., Görlich, A., Zander, J.F., Ahnert-Hilger, G., and Ibañez-Tallon, I. (2015). An essential role of acetylcholine-glutamate synergy at habenular synapses in nicotine dependence. *eLife* 4, e11396. <https://doi.org/10.7554/eLife.11396>.
56. Souter, E.A., Chen, Y.-C., Zell, V., Lallai, V., Steinkellner, T., Conrad, W.S., Wisden, W., Harris, K.D., Fowler, C.D., and Hnasko, T.S. (2022). Disruption of VGLUT1 in cholinergic medial habenula projections increases nicotine self-administration. *eNeuro* 9, ENEURO.0481-21.2021. <https://doi.org/10.1523/ENEURO.0481-21.2021>.
57. Brischoux, F., Chakraborty, S., Brierley, D.I., and Ungless, M.A. (2009). Phasic excitation of dopamine neurons in ventral VTA by noxious stimuli. *Proc. Natl. Acad. Sci. USA* 106, 4894–4899. <https://doi.org/10.1073/pnas.0811507106>.
58. Ungless, M.A., Magill, P.J., and Bolam, J.P. (2004). Uniform inhibition of dopamine neurons in the ventral tegmental area by aversive stimuli. *Science* 303, 2040–2042. <https://doi.org/10.1126/science.1093360>.
59. Matsumoto, M., and Hikosaka, O. (2009). Two types of dopamine neuron distinctly convey positive and negative motivational signals. *Nature* 459, 837–841. <https://doi.org/10.1038/nature08028>.
60. Hnasko, T.S., Hjelmstad, G.O., Fields, H.L., and Edwards, R.H. (2012). Ventral tegmental area glutamate neurons: electrophysiological properties and projections. *J. Neurosci.* 32, 15076–15085. <https://doi.org/10.1523/JNEUROSCI.3128-12.2012>.
61. Taylor, S.R., Badurek, S., Dileone, R.J., Nashmi, R., Minichiello, L., and Picciotto, M.R. (2014). GABAergic and glutamatergic efferents of the mouse ventral tegmental area. *J. Comp. Neurol.* 522, 3308–3334. <https://doi.org/10.1002/cne.23603>.
62. Faure, A., Reynolds, S.M., Richard, J.M., and Berridge, K.C. (2008). Mesolimbic dopamine in desire and dread: enabling motivation to be generated by localized glutamate disruptions in nucleus accumbens. *J. Neurosci.* 28, 7184–7192. <https://doi.org/10.1523/JNEUROSCI.4961-07.2008>.
63. Richard, J.M., and Berridge, K.C. (2011). Nucleus accumbens dopamine/glutamate interaction switches modes to generate desire versus dread: D(1) alone for appetitive eating but D(1) and D(2) together for fear. *J. Neurosci.* 31, 12866–12879. <https://doi.org/10.1523/JNEUROSCI.1339-11.2011>.
64. Zweifel, L.S., Fadok, J.P., Argilli, E., Garelick, M.G., Jones, G.L., Dickerson, T.M.K., Allen, J.M., Mizumori, S.J.Y., Bonci, A., and Palmiter, R.D. (2011). Activation of dopamine neurons is critical for aversive conditioning and prevention of generalized anxiety. *Nat. Neurosci.* 14, 620–626. <https://doi.org/10.1038/nn.2808>.
65. Fadok, J.P., Dickerson, T.M.K., and Palmiter, R.D. (2009). Dopamine is necessary for cue-dependent fear conditioning. *J. Neurosci.* 29, 11089–11097. <https://doi.org/10.1523/JNEUROSCI.1616-09.2009>.
66. Kramer, D.J., Aisenberg, E.E., Kosillo, P., Friedmann, D., Stafford, D.A., Lee, A.Y.-F., Luo, L., Hockemeyer, D., Ngai, J., and Bateup, H.S. (2021). Generation of a DAT-P2A-Flpo mouse line for intersectional genetic targeting of dopamine neuron subpopulations. *Cell Rep.* 35, 109123. <https://doi.org/10.1016/j.celrep.2021.109123>.



67. Gore, B.B., Soden, M.E., and Zweifel, L.S. (2013). Manipulating gene expression in projection-specific neuronal populations using combinatorial viral approaches. *Curr. Protoc. Neurosci.* 65, 4.35.1–4.3520. <https://doi.org/10.1002/0471142301.ns0435s65>.
68. Grimm, D., Kern, A., Rittner, K., and Kleinschmidt, J.A. (1998). Novel tools for production and purification of recombinant adenoassociated virus vectors. *Hum. Gene Ther.* 9, 2745–2760. <https://doi.org/10.1089/hum.1998.9.18-2745>.
69. Fenno, L.E., Ramakrishnan, C., Kim, Y.S., Evans, K.E., Lo, M., Vesuna, S., Inoue, M., Cheung, K.Y.M., Yuen, E., Pichamoorthy, N., et al. (2020). Comprehensive dual- and triple-feature intersectional single-vector delivery of diverse functional payloads to cells of behaving mammals. *Neuron* 107, 836–853.e11. <https://doi.org/10.1016/j.neuron.2020.06.003>.
70. Chen, T.-W., Wardill, T.J., Sun, Y., Pulver, S.R., Renninger, S.L., Baohan, A., Schreiter, E.R., Kerr, R.A., Orger, M.B., Jayaraman, V., et al. (2013). Ultrasensitive fluorescent proteins for imaging neuronal activity. *Nature* 499, 295–300. <https://doi.org/10.1038/nature12354>.
71. Ting, J.T., Lee, B.R., Chong, P., Soler-Llavina, G., Cobbs, C., Koch, C., Zeng, H., and Lein, E. (2018). Preparation of acute brain slices using an optimized N-methyl-D-glucamine protective recovery method. *J. Vis. Exp.* 132. <https://doi.org/10.3791/53825>.

## STAR★METHODS

### KEY RESOURCES TABLE

REAGENT or RESOURCE	SOURCE	IDENTIFIER
<b>Antibodies</b>		
Sheep anti-TH	Pelfreeze	RRID: AB_461070
Rabbit anti-GFP	Invitrogen	RRID: AB_221569
Chicken anti-GFP	Invitrogen	RRID: AB_2534023
Rabbit anti-HA	Sigma Aldrich	RRID: AB_260070
Alexa Fluor 488-AffiniPure Donkey Anti-Rabbit	Jackson ImmunoResearch	RRID: AB_2313584
Alexa Fluor 647-AffiniPure Donkey Anti-Sheep	Jackson ImmunoResearch	RRID: AB_2340751
Alexa Fluor 488-AffiniPure F(ab') <sub>2</sub> Fragment Donkey Anti-Chicken	Jackson ImmunoResearch	RRID: AB_2340376
Alexa Fluor 594-AffiniPure F(ab') <sub>2</sub> Fragment Donkey Anti-Rabbit IgG	Jackson ImmunoResearch	RRID: AB_2340622
<b>Bacterial and virus strains</b>		
AAV1-FLEX-ChR2-EYFP	Hunker et al. <sup>25</sup>	N/A
AAV1-FLEX-EYFP	Hunker et al. <sup>25</sup>	N/A
AAV1-FLEX-SaCas9-Ug-sgVglut2	Hunker et al. <sup>25</sup>	N/A
AAV1-FLEX-SaCas9-U6-sgTh	Hunker et al. <sup>25</sup>	N/A
AAV1-FLEX-SaCas9-U6-sgRosa26	Hunker et al. <sup>25</sup>	N/A
AAV5-hSyn-Flex-GCaMP6f	Chen et al. <sup>70</sup>	RRID: Addgene 100833
AAV8-EF1a-Con/Fon-GCaMP6f	Fenno et al. <sup>69</sup>	RRID: Addgene 137122
<b>Chemicals, peptides, and recombinant proteins</b>		
6,7-dinitroquinoxaline-2,3-dione (DNQX)	Sigma-Aldrich	Cat# 0540
Dopamine hydrochloride	Alfa Aesar	Cat# A11136
Sodium Azide	Fisher Scientific	Cat# S2271
Dihydro-β-erythroidine hydrobromide (DhβE)	Tocris	Cat# 2349
<b>Experimental models: Organisms/strains</b>		
<i>Slc17a6</i> <sup>+/-Cre</sup> (VGLUT2cre)	Jackson Laboratories	RRID: IMSR_JAX:016963
<i>Slc6a3em1</i> (flpo)Hbat DAT flp	Kramer et al. <sup>66</sup>	RRID: IMSR_JAX:035436
<b>Software and algorithms</b>		
Illustrator	Adobe	RRID: SCR_010279
pClamp software V10	Molecular Devices	RRID: SCR_011323
Prism V6	GraphPad Software	RRID: SCR_002798
AnyMaze V6	Stoelting	RRID: SCR_014289
Synapse	TDT	N/A
TarHeel CV	Mark Wightman	N/A
Fiber photometry analysis	This paper	Figshare: <a href="https://doi.org/10.6084/m9.figshare.23556981">https://doi.org/10.6084/m9.figshare.23556981</a>
<b>Other</b>		
Nanoject III	Drummond Scientific	Cat#:3-000-207
Small Animal Stereotaxic Instrument with Digital Display Console, Model 940	David Kopf Instruments	N/A
Leica Cryostat	Leica	Cat#:CM-3050S
Pipette puller PC-100	Narishige	N/A
Leica Vibratome VT1200	Leica	RRID: SCR_018453

(Continued on next page)

## Continued

REAGENT or RESOURCE	SOURCE	IDENTIFIER
Axio examiner	Zeiss	RRID: SCR_018876
Multiclamp 700B Amplifier	Axon instruments	RRID: SCR_018455
RZ5 Processor	TDT	N/A

## RESOURCE AVAILABILITY

### Lead contact

Further information and requests for resources and reagents should be directed to and will be fulfilled by the lead contact (Thomas Hnasko: [thnasko@health.ucsd.edu](mailto:thnasko@health.ucsd.edu)).

### Materials availability

This study did not generate new unique reagents.

### Data and code availability

- All data reported in this paper will be shared by the [lead contact](#) upon request.
- All original code has been deposited at Github repository and is publicly available as of the date of publication. DOIs are listed in the [key resources table](#).
- Any additional information required to reanalyze the data reported in this paper is available from the [lead contact](#) upon request.

## EXPERIMENTAL MODEL AND STUDY PARTICIPANT DETAILS

Male and female mice were bred at University of California San Diego (UCSD) and group-housed on a 12-hour light/dark cycle, with food and water *ad libitum* unless otherwise noted. *Slc17a6<sup>+/-Cre</sup>* (VGLUT2-Cre) mice were initially obtained from Jackson Laboratory (Stock: 016963) and maintained back-crossed on to C57BL/6J. DAT<sup>+/-Flp</sup> mice were initially obtained from Dr. Helen Bateup (UC Berkeley),<sup>66</sup> and crossed to VGLUT2-Cre mice to generate a dual transgenic, DAT-Flp/VGLUT2-Cre line. All experiments were performed on mice at least 6 weeks of age and in accordance with protocols approved by UCSD Institutional Animal Care and Use Committee.

## METHOD DETAILS

### Viral production

Production of AAV1 (AAV1-FLEX-ChR2-EYFP, AAV1-FLEX-EYFP, AAV1-FLEX-SaCas9-Ug-sgVglut2, AAV1-FLEX-SaCas9-U6-sgTh, and AAV1-FLEX-SaCas9-U6-sgRosa26) were as previously described.<sup>67</sup> Briefly, pAAV shuttle plasmids were co-transfected with the packaging plasmid pDG1<sup>68</sup> into HEK293T/17 cells (ATCC) and viral particles were purified by cesium chloride gradient centrifugation. Viral particles were resuspended in Hank's balanced saline solution and titers were calculated using gel electrophoresis and densitometry against a known standard.

### Stereotactic surgeries

Mice > 6 weeks old were anesthetized with isoflurane (4% for induction; 1-2% maintenance) and placed in a stereotaxic frame (Kopf Instruments). For CRISPR/Cas9 experiments AAV vectors were made in-house (Zweifel lab) as described.<sup>25</sup> AAV1-FLEX-ChR2-EYFP ( $8 \times 10^{12}$  vg/mL) was combined with either AAV1-FLEX-SaCas9-U6-sgVglut2 ( $1.5 \times 10^{12}$  vg/mL), AAV1-FLEX-SaCas9-U6-sgTh ( $1.8 \times 10^{12}$  vg/mL), or AAV1-FLEX-SaCas9-U6-sgRosa26 ( $1.5 \times 10^{12}$  vg/mL) such that ChR2-YFP constituted 1/7<sup>th</sup> of the total volume and the respective SaCas9 constituted 6/7<sup>th</sup> of the total volume. 400nL of this mixture was injected into the VTA of VGLUT2-cre mice (Distance from Bregma in mm: -3.4 AP; +0.35 ML; -4.4 DV) at 100nL/min using a glass pipette attached to a microinjector (Nanoject 3, Drummond Scientific). Following viral infusion, the injector tip was kept in place for 10 min before slowly retracting. For optogenetic self-stimulation experiments, optic fibers (200μm core; Newdoon) were subsequently placed bilaterally above NAc medial shell at a 10° medio-lateral angle (+1.4 AP; ±1.13 ML; -3.81 DV). Optic fibers were secured with 2-4 skull screws and dental cement (Lang Dental Mfg).

For fiber photometry experiments, 400nL of AAV5-hSyn-Flex-GCaMP6f ( $1.05 \times 10^{13}$  vg/mL; Addgene 100833) was injected into the VTA of VGLUT2-Cre mice (same coordinates as above) to target GCaMP expression to VTA glutamate neurons or, in separate mice, 400 nL of AAV8-EF1a-Con/Fon-GCaMP6f ( $1.15 \times 10^{13}$  vg/mL; Addgene 137122<sup>69</sup>) was injected into VTA of VGLUT2-Cre/DAT-Flp mice to selectively target glutamate neurons that co-release dopamine. Wildtype, VGLUT2-Cre, or DAT-Flp only mice were also injected with AAV8-EF1a-Con/Fon-GCaMP6f and assessed for non-selective expression to confirm specificity of virus and Cre/Flp

expression.<sup>70</sup> We also confirmed by TH IHC that expression of GCaMP was concentrated in TH+ neurons in DAT-Flp/VGLUT2-Cre mice ( $99.2 \pm 0.4\%$  of GCaMP+ neurons were TH+; 237 out of  $239 \pm 53$  GCaMP+ neurons;  $n=5$  mice) and that a smaller proportion of GCaMP labeled cells were TH+ in the VGLUT2-Cre mice ( $11.3 \pm 3\%$  of GCaMP+ neurons were TH+; 47 out of  $415 \pm 30$  GCaMP+ neurons;  $n=5$  mice) (Figure S1A). An optic fiber (400 $\mu$ m core; Doric) was placed above VTA (Distance from Bregma in mm: -3.4 AP; +0.35 ML; -4.2 DV) then secured with 2-4 skull screws and dental cement. Mice were treated with topical antibiotic and with carprofen (5mg/kg; s.c.; Rimadyl) immediately following surgery and 24 hr later. Mice were allowed 6 weeks for recovery before experiments began.

### Immunohistochemistry

Mice were deeply anesthetized with sodium pentobarbital (200mg/kg i.p.; VetOne) and transcardially perfused with 30-40 mL of phosphate-buffered saline (PBS) followed by 60-70 mL of 4% paraformaldehyde (PFA) at  $\sim 7$  mL/min. Brains were extracted and stored in 4% PFA overnight, followed by cryoprotection in 30% sucrose for 48-72 hr at 4°C. Brains were subsequently flash frozen in isopentane and stored at -80°C. 30- $\mu$ m sections were cut using a cryostat (Leica) and stored in PBS containing 0.01% sodium azide. For immunostaining, sections were blocked with 4% normal donkey serum (Jackson ImmunoResearch) in PBS containing 0.2% Triton-X 100 for 1 hour at room temperature. Sections were then incubated in sheep anti-TH (1:2000; Pelfreeze P60101-0) and rabbit anti-GFP (1:2000; Invitrogen A11122), or chicken anti-GFP (1:2000; Invitrogen A10262) and rabbit anti-HA (to stain for HA tag present on CRISPR/Cas9 vectors; 1:2000; Sigma H6908) overnight at 4°C. Following primary incubation, sections were rinsed in PBS 3 times for 10 min each and subsequently incubated in secondary antibodies conjugated to Alexa 488 (Donkey anti-rabbit; 1:400) and Alexa 647 (Donkey anti-sheep; 1:400), or Alexa 488 (Donkey anti-chicken; 1:400) and Alexa 594 (Donkey anti-rabbit; 1:400) (Jackson ImmunoResearch) for 2 hr at room temperature. Sections were then rinsed in PBS 3 times for 10 min each, mounted onto glass slides, and coverslipped with Fluoromount-G mounting medium (Southern Biotech) containing 0.5 $\mu$ g/mL DAPI (Sigma).

Images were taken using a widefield epifluorescent microscope (Zeiss AxioObserver). Tiled images were taken at 10x magnification using appropriate filters and identical acquisition settings across all slides. Approximately 3-4 sections through rostral-caudal extent of VTA and 3-4 sections from NAc were imaged. Spread of ChR2 expression and optic fiber placements were mapped onto corresponding coronal sections in the Paxinos Mouse Brain Atlas using Adobe Illustrator (Version 23). Mice were excluded from experiments if there was substantial spread of ChR2 terminal expression outside of NAc (beyond 10% total volume), for example in septal regions ( $n=2$ ).

### Electrophysiological recordings in mouse brain slices

Adult mice 12-14 weeks old were deeply anesthetized with sodium pentobarbital (200mg/kg; i.p.; VetOne) and transcardially perfused with 15 mL ice-cold NMDG artificial cerebro-spinal fluid (aCSF) containing (in mM): 92 NMDG, 2.5 KCl, 1.25 NaH<sub>2</sub>PO<sub>4</sub>, 30 NaHCO<sub>3</sub>, 20 HEPES, 25 D-Glucose, 2 thiourea, 5 Na-ascorbate, 3 Na-pyruvate, 0.5 CaCl<sub>2</sub>, and 10 MgSO<sub>4</sub>, and continuously bubbled with carbogen (95% O<sub>2</sub> + 5% CO<sub>2</sub>). Brains were then extracted and 200- $\mu$ m coronal slices were cut using a vibratome (Leica) containing ice-cold NMDG-aCSF. Slices were then transferred to a recovery chamber containing NMDG-aCSF at 31°C for 20-30 min. A 2M Na<sup>+</sup> spike-in solution (116mg/mL Na<sup>+</sup> in NMDG-aCSF) was added to the recovery chamber in increasing volumes (from 250 $\mu$ L to 1mL) in 5 min increments for 25 min in order to achieve a controlled rate of reintroduction of Na<sup>+</sup> into the chamber.<sup>71</sup> 5 min after the last Na<sup>+</sup>-spiking solution, slices were then transferred into room temperature HEPES-aCSF containing (in mM): 92 NaCl, 2.5 KCl, 1.25 NaH<sub>2</sub>PO<sub>4</sub>, 30 NaHCO<sub>3</sub>, 20 HEPES, 25 D-Glucose, 2 thiourea, 5 Na-ascorbate, 3 Na-pyruvate, 2 CaCl<sub>2</sub>, 2 MgSO<sub>4</sub>, and continuously bubbled in carbogen. After >45 min recovery, slices were transferred to a recording chamber continuously perfused with carbogenated aCSF (in mM: 124 NaCl, 2.5 KCl, 1.25 NaH<sub>2</sub>PO<sub>4</sub>, 24 NaHCO<sub>3</sub>, 5 HEPES, 12.5 D-Glucose, 2 CaCl<sub>2</sub>, 2 MgSO<sub>4</sub>) at a rate of 2-3 mL/min and maintained at 32°C by an in-line heater (Warner Instruments).

Patch-pipettes (4.5-7 M $\Omega$ ) were pulled from borosilicate glass (Kings Precision Glass) using a gravity puller (Narishige). Pipettes were filled with a cesium-based internal solution containing (in mM): 130 D-Gluconic acid, 130 CsOH, 5 NaCl, 10 HEPES, 12 phosphocreatine, 3 Mg-ATP, 0.2 Na-GTP, 10 EGTA, at pH 7.25 and 285 mOsm. Epifluorescence was used to locate YFP-labelled VGLUT2 VTA terminals in NAc medial shell and subsequent visually guided patch recordings were made using infrared differential interference contrast (IR-DIC) illumination (A1 Examiner, Zeiss). A light-emitting diode (UHP-LED460, Prizmatix) under computer control was used to flash blue light through the light path of the microscope to activate ChR2. Recordings were made in whole cell voltage clamp using a Multiclamp 700B Amplifier (Axon Instruments), filtered at 2 kHz, and digitized at 10 kHz (Axon Digidata, Axon Instruments), and collected using pClamp v10 software (Molecular Devices). Capacitance and series resistance were electronically corrected before recordings, and series resistance was monitored throughout recordings. Any cell in which series resistance changed >20% was discarded and excluded from analyses.

To record excitatory postsynaptic currents (EPSCs), neurons were voltage clamped at -70 mV in whole cell configuration. A single 5-ms blue light pulse was applied every 45 s, and 10 light-evoked currents were averaged per neuron per condition. AMPA ( $\alpha$ -amino-3-hydroxy-5-methyl-4-isoxazolepropionic acid) receptors were blocked using 6,7-dinitroquinoxaline-2,3-dione (DNQX, Sigma) dissolved in dimethyl sulfoxide and diluted by 1000 in aCSF for 10 $\mu$ M bath application. To record intrinsic membrane properties in VTA, pipettes were filled with (in mM): 130 K-gluconate, 2 KCl, 2 MgCl<sub>2</sub>, 2 Na<sub>2</sub>-ATP, 0.3 Na-GTP, 10 phosphocreatine, 10 HEPES and 0.2 EGTA, adjusted to a pH of 7.3 and 280 mOsm. Whole cell patch clamp recordings were made from ChR2:eYFP positive neurons in the medial VTA (those that evoked fast photocurrents in response to a single 5 ms or 500 ms blue light pulse). Resting membrane voltage



and spontaneous firing was measured in current clamp at 0 pA immediately after entering whole-cell mode. The resting membrane voltage was corrected for the liquid junction potential (LJP) calculated as 15.2 mV using pClamp. Input resistance and capacitance were measured in voltage-clamp in response to a 200 ms -10 mV voltage step.  $I_h$  was calculated in voltage clamp in response to a voltage step from -60 mV to -110 mV. Cell firing frequency was determined in response to a 500 ms square current step incremented by 20 pA every sweep.

### ***In vitro* fast-scan cyclic voltammetry recordings**

Coronal slices from adult mice were prepared as above with the exception that slices were cut to 300  $\mu$ m thickness. Carbon fiber electrodes were prepared using 7  $\mu$ M thick carbon fiber threaded through glass pipettes. Pipettes were pulled to seal around the carbon fiber, and subsequently cut so that  $\sim$ 100  $\mu$ m of carbon fiber was exposed beyond the pipette. Pipettes were backfilled with 3M KCl, and a Ag/AgCl reference electrode was also placed in the recording chamber. The potential of the carbon fiber electrode was held at -0.4 V versus reference, ramped to 1.3 V, and back to -0.4 V at 400 V/s. This triangular waveform was first applied at 60 Hz for 10–15 min in the bath, and then at 10 Hz for the duration of slice recordings. Dopamine transients were evoked optogenetically applied through the light path of the microscope as above, in 1-s train at 20 Hz frequency and 1 Hz (single 5ms pulse). Optogenetic stimulations were applied every 2 min, with four repetitions for each frequency. In a separate experiment, optogenetic stimulations at 20 Hz were delivered every 2 min for 10 repetitions, and nicotinic receptor antagonist Dihydro- $\beta$ -erythroidine hydrobromide (DH $\beta$ E; 1  $\mu$ M, Tocris) was applied during the last 6 repetitions. Data were collected and analyzed using TarheelCV software. The amplitude of evoked dopamine transients were measured at the site of peak oxidation (0.6–0.7 V), and averaged across 3 recordings for each frequency or across the last 3 recordings of each drug condition. To estimate dopamine concentration, each electrode was calibrated to 1000 nM dopamine (Alfa Aesar A11136) prepared fresh daily.

### **Fiber photometry recordings**

For all fiber photometry experiments, mice were tethered to a 50 or 100 cm-long patch cord (400  $\mu$ m core, NA 0.48, Doric) attached to a pigtailed fiber optic rotary joint (Doric) connected through a FC connector to dichroic mirrors (minicube, Doric) and then to an LED driver (Doric). An isosbestic channel (405nm) was used to control for movement artifacts while 465nm was used to stimulate GCaMP. Fluorescence was transmitted through a femtowatt photodetector (Newport, Doric), digitized at 1017 Hz, recorded by a real-time signal processor (RZ5P, TDT), and processed by Synapse software (TDT). Behavioral and event timestamps were integrated by TTL inputs from Med-PC, Any-Maze, or manual triggers. Analysis of the recorded calcium signals was performed using custom-written MATLAB scripts.

Fluorescent signal in the isosbestic channel was fitted to the signal at 465nm, and then subtracted from the 465nm signal to create a  $\Delta F/F$  (dF/F). dF/F was monitored over a baseline, pre-stimulus window of 5s, followed by 10s post-stimulus and subsequently normalized to z-score based on the mean and standard deviation of the 5s baseline dF/F. Peak z-score (highest absolute value) at the time of event (0 to 1s) were then extracted per animal and averaged per group. Significance of peak z-score was assessed within each treatment group compared to a mean of zero using one-sample t-tests.

Behavioral experiments during fiber photometry recordings occurred in the order described below.

### **Pavlovian conditioned approach**

Mice were food restricted to 85–90% baseline weight. One day before testing, mice were exposed to sucrose pellets in their home cage. During testing, mice were placed into operant chambers (Med Associates), equipped with one lever on either side of a magazine containing a food dish, and controlled by MedPC IV software. On day 1 of testing, sucrose pellets were non-contingently delivered on a variable interval of 60 sec into the magazine. Starting day 2, Pavlovian conditioning began. During each conditioning trial, a CS+ lever was presented for 5 sec, followed immediately by sucrose pellet delivery into the magazine. Magazine entries during the CS+, immediately following the CS+, and throughout the whole session were recorded, as well as lever presses during CS+ trials. There were 15 trials per session, occurring on a 60 sec variable interval. Mice were conditioned for 5 days. On Day 5, however, 50% of CS+ lever presentations resulted in an omission of sucrose pellet delivery.

### **Instrumental sucrose task**

Mice were placed into operant chambers (MedAssociates), equipped with two levers on either side of a magazine containing a food dish, and controlled by MedPC IV software. At the beginning of a session, house lights and LED cue lights above each lever were turned on. Lever presses at the active lever delivered a sucrose pellet (20 mg, BioServ F0071) into the food dish at a fixed ratio 1 and turned off the LED cue light for 1 s. Lever presses at the other, inactive lever, were recorded but had no consequence. Active lever location was the same across days for each mouse, but counterbalanced between mice. Sessions lasted 30 min.

### **Looming stimulus**

Mice were placed in an open field apparatus (45 cm W x 45 cm D x 40 cm H) on a baseline day for 11 min. On a following test day mice were placed in the same open field apparatus and the first three minutes served as a baseline period. After which, a looming stimulus (black cardboard circle, 15 cm diameter) attached to a handle was lowered above the center of the apparatus for approximately 1 sec, once per minute for a total of 8 trials.

### **Cue-footshock conditioning**

Mice were placed in operant chambers equipped with shock generator, grid floor, house light, and sound generator (Med Associates). During the first day, the first 3 minutes of the session served as a baseline period for the mouse to acclimate to the chamber.

After 3 min, a 5 s tone (CS+) was presented and immediately followed by delivery of 0.5 mA footshock (UCS). Mice were exposed to 10 tone-shock pairings on a 45–60 s variable inter-trial interval. The following day, day 2, mice were placed in the same chamber but in slightly changed context with plexiglass floor and no house light. After a 3 min baseline period, mice were exposed to 10 tone CS+ presentations without any footshock (UCS) delivery.

## **2 nose-poke optogenetic self-stimulation procedure**

Mice were food restricted to 85–90% baseline body weight prior to and during testing to increase baseline responding. Mice were tethered to a 50 cm patch cable attached to an optical rotary joint (Doric), connected through an FC connector to laser (473 nm, Shanghai Laser & Optics Century). Mice were placed in operant chambers (Med Associates) controlled by MedPC IV software. The beginning of each session turned on the house light, played a 0.5 s tone (2 kHz), and turned on LED cue lights located over each of the 2 nose ports. Each nose port contained photobeams and were baited with one 20 mg sucrose pellet (BioServ F0071) prior to each session. Beam breaks into each nose port ('nose poke') triggered a 0.5 s tone and turned off the LED cue lights for 1 s. Beam breaks into the active nose port also delivered laser stimulation (1 s, 10 mW, 40 Hz, 5 ms pulse width) through a TTL-generator controlled by an Arduino board. Nose pokes that occurred during the 1 s laser stimulation were recorded but had no consequence. Sessions lasted 45 min. Starting on day 5 of testing, the active nose port delivering laser stimulation was switched to the opposite nose port location (formerly the inactive nose port) until testing ended on day 8.

## **Real-time place preference/avoidance procedure**

Mice were tethered to a patch cable attached to an optical rotary joint (Doric) connected to a laser. During a baseline (no-laser) session, mice were placed on the border between two adjoining homogenous grey compartments (20 x 20 cm each). The amount of time spent in each compartment as well as entries into each compartment were recorded using AnyMaze software (v6; San Diego Instruments). Most mice did not display a side preference, but any mice displaying a >75% side preference during the baseline session were excluded from further study ( $n=0$ ). Starting on day 2, one side was designated active, wherein entries triggered laser stimulation (continuous, 473 nm, 10 mW, 40 Hz, 5 ms pulse width) controlled by AnyMaze software. Sessions lasted 20 min, and on days 5–7 the active (laser-delivering) compartment was switched.

## **Open Field**

Mice were placed into an open field (45 cm W x 45 cm D x 40 cm H) for 20-min sessions. Distance travelled, time in center, and number of entries into the center of the apparatus were collected using AnyMaze software. In a separate session, laser stimulation (473 nm, 40 Hz frequency) was delivered during a 6 min session, for the last 3 min of the session.

## **QUANTIFICATION AND STATISTICAL ANALYSIS**

Data were analyzed using Student's *t*-test, 2-way repeated-measure ANOVA followed by Bonferroni post-hoc multiple comparisons, one-way ANOVAs followed by Tukey, Sidak, or Dunnett post-hoc multiple comparisons, or Pearson correlation (GraphPad Prism v6). All data are represented as mean  $\pm$  standard error of the mean (SEM) and/or as individual points. All statistical details of experiments, including statistical tests used and sample sizes, can be found in results and in figure legends.